Monthly Notices of the ROYAL ASTRONOMICAL SOCIETY

MNRAS **522,** 1358–1376 (2023) https://doi.org/10.1093/mnras/stad936
Advance Access publication 2023 March 30

A critique of the Spite Plateau and the astration of primordial lithium

J. E. Norris,[1]★ D. Yong,[1,2] A. Frebel[3] and S. G. Ryan[4]

[1] *Research School of Astronomy and Astrophysics, Australian National University, Canberra, ACT 0200, Australia*
[2] *ARC Centre of Excellence for Astrophysics in Three Dimensions (ASTRO-3D), Australia*
[3] *Department of Physics and Kavli Institute for Astrophysics and Space Research, Massachusetts Institute of Technology, Cambridge, MA 02139, USA*
[4] *Department of Physics, Astronomy and Mathematics, University of Hertfordshire, College Lane, Hatfield AL10 9AB, UK*

Accepted 2023 March 10. Received 2023 March 6; in original form 2022 December 3

ABSTRACT

We investigate the distribution of the lithium abundances, A(Li), of metal-poor dwarf and subgiant stars within the limits 5500 K $< T_{\rm eff} <$ 6700 K, $-6.0 <$ [Fe/H] < -1.5, and log $g \gtrsim 3.5$ (a superset of parameters first adopted by Spite and Spite), using literature data for some 200 stars. We address the problem of the several methods that yield $T_{\rm eff}$ differences up to 350 K, and hence uncertainties of 0.3 dex in [Fe/H] and A(Li), by anchoring $T_{\rm eff}$ to the infrared flux method. We seek to understand the behaviour of A(Li) as a function of [Fe/H] – small dispersion at highest [Fe/H], 'meltdown' at intermediate values (i.e. large spread in Li below the Spite Plateau), and extreme variations at lowest [Fe/H]. Decreasing A(Li) is accompanied by increasing dispersion. Insofar as [Fe/H] increases as the Universe ages, the behaviour of A(Li) reflects chaotic star formation involving destruction of primordial Li, which settles to the classic Spite Plateau, with A(Li) $\sim$ 2.3, by the time the Galactic halo reaches [Fe/H] ~ -3.0. We consider three phases: (1) first star formation in C-rich environments ([C/Fe] > 2.3), with depleted Li; (2) silicates-dominated star formation and destruction of primordial Li during pre-main-sequence evolution; and (3) materials from these two phases co-existing and coalescing to form C-rich stars with A(Li) below the Spite Plateau, leading to a toy model with the potential to explain the 'meltdown'. We comment on the results of Mucciarelli et al. on the Lower RGB, and the suggestion of Aguado et al. favouring a lower primordial lithium abundance than generally accepted.

Key words: stars: abundances – stars: Population II – Galaxy: abundances – early Universe.

1 INTRODUCTION

One of the basic predictions of the Big Bang cosmological model is that lithium is produced in a hot Big Bang (Wagoner, Fowler & Hoyle 1967; Wagoner 1973). Subsequently, Spite & Spite (1982) first reported the small dispersion in lithium abundances in near-main-sequence stars in the ranges 5500 K $< T_{\rm eff} <$ 6500 K and $-2.4 <$ [Fe/H][1] < -1.1 (later to be known as the Spite Plateau) and proposed these stars as potential probes of the Big Bang prediction. They reported a lithium abundance of the Spite Plateau of A(Li) $= 2.05 \pm 0.15$; but also noted, 'The observed lithium abundance is thus at least a lower limit of the ^{7}Li produced by the Big Bang'. Two decades later, after considerable further investigation of the properties of the Big Bang and the Spite Plateau, by many investigators, it became clear there is indeed a significant difference between theory and observation as documented, for example, by Cyburt, Fields & Olive (2008), who reported a predicted primordial lithium abundance [based on Wilkinson Microwave Anisotropy Probe (WMAP; Dunkley et al. 2009) and Big Bang ΛCDM cosmology][2] of A(Li)$_{\rm P}$ $= 2.72 \pm 0.06$ and the Spite Plateau value of A(Li) $= 2.09 \pm 0.16$ for near-main-sequence stars – a difference of 0.63 ± 0.17 dex. This was referred to as 'The Lithium Problem'.

The situation, however, became considerably more challenging as it became clear that many dwarfs of lower metallicity in the range $-6.0 <$ [Fe/H] < -2.5 (and ages most likely closer to that of the Big Bang) have lithium abundances considerably smaller than A(Li) $= 2.0$. The majority of the seven known dwarfs with [Fe/H] < -4.5 have $2.0 <$ A(Li) < 0.5 (beginning with HE 1327 − 2326, which has [Fe/H] $= -5.6$ and A(Li) < 1.6 (Frebel et al. 2005); and in the range $-4.0 <$ [Fe/H] < -3.0, Sbordone et al. (2010) and Bonifacio et al. (2012) reported a 'meltdown' of the Spite Plateau, once again involving near-main-sequence stars with A(Li) values considerably less than 2.0.

Table 1 presents a brief list of some 20 important milestones (including those above) relevant to the investigations of Li abundances, which have played an important role in our current understanding of the early Universe.

★ E-mail: john.norris@anu.edu.au

[1]Throughout this paper, stellar chemical abundances assume 1D,LTE (one-dimension, local-thermodynamic-equilibrium) modelling, unless otherwise stated.

[2]We note the Planck Collaboration VI (2020) result: 'We do not discuss other light elements, such as... lithium, since the observed abundance measurements and their interpretation in terms of the standard models of BBN are more controversial [see Fields (2011), Fields, Molaro & Sarkar (2014), for reviews]. The Planck results do not shed any further light on these problems compared to earlier CMB experiments'.

© 2023 The Author(s).
Published by Oxford University Press on behalf of Royal Astronomical Society. This is an Open Access article distributed under the terms of the Creative Commons Attribution License (http://creativecommons.org/licenses/by/4.0/), which permits unrestricted reuse, distribution, and reproduction in any medium, provided the original work is properly cited.

Downloaded from https://academic.oup.com/mnras/article/522/1/1358/7095871 by guest on 27 April 2025

Table 1. Major milestones in the study of lithium abundances in the metal-poor near-main-sequence stars.

Milestone	Authors[1]
Prediction of lithium production in the early stages of a homogeneous and isotropic expanding Universe	WA67, WA73
Discovery of the Spite Plateau: $\langle A(Li)\rangle = 2.05$, for stars with 5500 K $< T_{\rm eff} <$ 6250 K, log $g \gtrsim 3.5$, and $-2.4 <$ [Fe/H] < -1.1	SP82
9 per cent of stars lie below the Plateau in the range $1.1 < A(Li) < 2.0$ ($T_{\rm eff} > 5800$ K, $-3.8 <$ [Fe/H] < -1.7)	TH94
The existence of 'rare cases of well-observed stars (with similar $T_{\rm eff}$ and [Fe/H] ~ -3.0) that cannot have the same Li abundance'	RY96
Spectra with S/N > 100 reveal the Spite Plateau (on the limited range 6100 K $< T_{\rm eff} <$ 6300 K) is slightly inclined with respect to [Fe/H]	RY99
Suggestion that 'ultra-Li-depleted halo stars and blue stragglers are manifestations of the same phenomenon'	RY01a, RY02
Discovery of HMP subgiant HE 1327–2326 with $[Fe/H]_{1D,\,LTE} = -5.66$ and $A(Li)_{1D,\,LTE} < 0.70$	FR05, AO06, FR08
Stellar model atmosphere computations establish $A(Li)_{3D,\,NLTE}$ and $A(Li)_{1D,\,LTE}$ values are essentially the same	AS03
Spectra with S/N > 300 yield Spite Plateau (5800 K $< T_{\rm eff} <$ 6400 K) slightly inclined over $-2.9 <$ [Fe/H] < -1.0	AS06
The Spite Plateau $\langle A(Li)\rangle = 2.09$ is lower than the WMAP and Big Bang ΛCDM primordial value $A(Li)_{\rm P} = 2.72$	CY08
Theoretical analysis of sensitivity of stellar atmospheric lithium abundances to standard stellar evolution modelling	DE90
Important theoretical suggestions to explain lower observed Spite Plateau A(Li) value: (a) Gravitational settling in the presence of weak turbulence in low-mass main sequence stars; (b) Depletion of Li by a first generation of stars; (c) Convective overshoot and residual mass accretion during pre-main-sequence and main-sequence evolution	RI05, PI06, FU15
The cooler $T_{\rm eff}$ limit of the Plateau moves to a higher value as [Fe/H] decreases	ME10
The components of the double-line binary CS22876-032 have different A(Li) = 2.22 and 1.75 ($T_{\rm eff} = 6500$, 5900 K and [Fe/H] $= -3.66, -3.57$)	TH94, GO08
Meltdown: large A(Li) spreads below the Spite Plateau value observed for [Fe/H] $\lesssim -3.0$	SB10, BO12, 15, 18
Discovery of most Fe-poor star SM 0313–6708[2], with [Fe/H] < -7.3 – a red giant deduced to have had main sequence $A(Li)_{\rm MS} \sim 2.0$	KE14, FR15
Spectra with S/N > 40–100 for 7 stars with $T_{\rm eff} > 5500$ K, log $g > 3.5$, and [Fe/H] < -3.5 yield $\langle A(Li)\rangle = 1.90$, with $\sigma = 0.10$	MA17a
At least 12 of the 14 stars known in 2019 to have [Fe/H] < -4.5 are C-rich, with [C/Fe] ≥ 0.7. 11 of them have [C/Fe] > 3.0	NO19
For the 8 stars having [Fe/H] < -4.5, log $g \gtrsim 3.5$, and lithium estimates, the mean lithium abundance is $\langle A(Li)\rangle \leq 1.5$	FR08,19, AG19, BO15,18, CA11,16, HA15, ST18
Suggestion that C enhancement and Li depletion are not directly related; 2 C-rich stars at [Fe/H] ~ -3.0 have normal A(Li)	MA17b
Lithium upper envelope over the range $-6.0 <$ [Fe/H] < -2.5 'nearly constant' at A(Li) ~ 2.0 suggests 'lower primordial production'	AG19
Discovery of a thin lithium plateau among metal-poor red giant branch stars	MU22

Notes. [1]WA67 = Wagoner et al. (1967), WA73 = Wagoner et al. (1967), SP82 = Spite & Spite (1982), TH94 = Thorburn (1994), RY96 = Ryan et al. (1996), RY99 = Ryan, Norris & Beers (1999), RY01a = Ryan et al. (2001a), RY02 = Ryan et al. (2002), FR05 = Frebel et al. (2005), AS06 = Asplund et al. (2006), FR08 = Frebel et al. (2008), AS03 = Asplund, Carlsson & Botnen (2003), CY08 = Cyburt et al. (2008; WMAP = Wilkinson Microwave Anisotropy Probe), DE90 = Deliyannis, Demarque & Kawaler (1990), RI05 = Richard, Michaud & Richer (2005), PI06 = Piau et al. (2006), FU15 = Fu et al. (2015), ME10 = Meléndez et al. (2010), GO08 = González Hernández et al. (2008), SB10 = Sbordone et al. (2010), BO12 = Bonifacio et al. (2012), BO15 = Bonifacio et al. (2015), BO18 = Bonifacio et al. (2018), KE14 = Keller et al. (2014), FR15 = Frebel & Norris (2015), MA17a = Matsuno et al. (2017a), NO19 = Norris & Yong (2019, see table 6), FR19 = Frebel et al. (2019), AG19 = Aguado et al. (2019), CA11 = Caffau et al. (2011), CA16 = Caffau et al. (2016), HA15 = Hansen et al. (2015), ST18 = Starkenburg et al. (2018), MA17b = Matsuno et al. (2017b), MU22 = Mucciarelli et al. (2022)
[2] SM 0313–6708 = SMSS J031300.36–670839.3.

The aim of the present work is threefold. First, we present a critique of the lithium abundances of near-main-sequence turnoff stars on the Spite Plateau (Spite & Spite 1982) in the range $-2.4 <$ [Fe/H] < -1.1, together with the observed followup that stretches down to [Fe/H] $= -6.0$. By way of closer introduction, Fig. 1 provides the background for discussion of what we see as five (not one) lithium problems. These are:

(1) the primordial 'Lithium Problem' discussed above – $A(Li)_{\rm P} = 2.72$, while $A(Li)_{\rm SpitePlateau} = 2.09$ (Cyburt et al. 2008);
(2) a sloping plateau (Ryan et al. 1999; Asplund et al. 2006);
(3) a group of stars with very low A(Li) values that exhibit relatively rapid rotation and appear to be related to 'blue stragglers' (Thorburn 1994; Ryan et al. 2001b 2002);
(4) the 'meltdown' of the plateau (Sbordone et al. 2010; Bonifacio et al. 2012 2015, 2018) referred to above; and
(5) the enormous range in A(Li) ($<0.5 <$ A(Li) < 2.0) among the most Fe-poor stars, with (in at least some cases) an anticorrelation between A(Li) and carbon abundance, [C/Fe].[3]

Secondly, having collated a literature data base of A(Li) values, we correct them to a common temperature scale by taking into account differences resulting from the various techniques adopted by authors – with a view to improving their relative accuracy. We also determine a further data set based on *ab initio* Infrared Flux Method (IRFM) temperatures, determined for stars having appropriate literature colours.

Thirdly, we examine the various physical processes noted in Table 1 that are potentially responsible for the 'problems' summarized in Fig. 1 for A(Li) values below that of the primordial value – that is, the

[3]We note that this paper does not consider the isotopic ratios of Li (on which there is also considerable literature debate).

Downloaded from https://academic.oup.com/mnras/article/522/1/1358/7095871 by guest on 27 April 2025

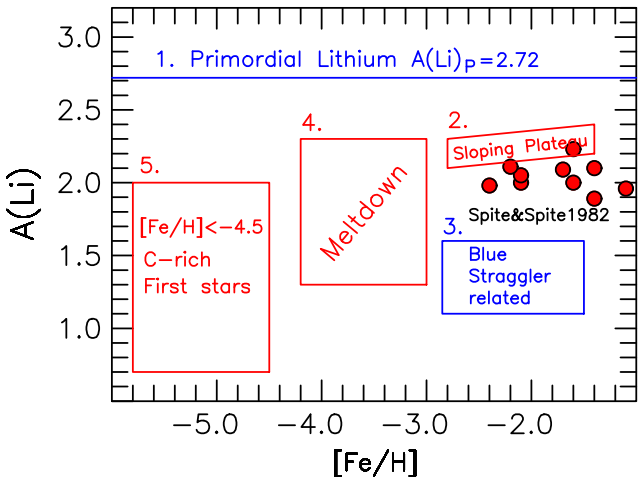

Figure 1. The five lithium problems. Red filled circles represent the original discovery data of Spite & Spite (1982).

phenomena responsible for the 'astration' of the primordial lithium. In particular, we follow the suggestions of Bromm & Loeb (2003), Frebel, Johnson & Bromm (2007), and Chiaki, Tominaga & Nozawa (2017), as well as references therein, concerning star formation in a C-rich environment to explain the stars with [Fe/H] < -4.5; and of Fu et al. (2015) on the astration of Li in C-normal stars in the range $-3.2 <$ [M/H] < -1.5 during their pre-main-sequence phase. In the range $-4.5 <$ [Fe/H] < -3.0, we then follow the suggestions of Norris et al. (2013) and Norris & Yong (2019) to investigate further the toy model they used to explain the fact that 20–30 per cent of stars with [Fe/H] < -2.0 are CEMP-no stars.[4] We shall argue that this model has the potential to explain the Sbordone et al. (2010), Bonifacio et al. (2012, 2015, 2018) 'meltdown' of the Spite Plateau.[5] In the appendix, we present a comparison between our conclusions with those presented by Mucciarelli et al. (2022) for stars on the lower red giant branch.

2 OBSERVATIONAL DATA

All lithium abundances in the present work are based on the Li I 6707 Å doublet. For our purposes, we compiled from the literature a catalogue of near-main-sequence stars having $T_{\rm eff}$, log g, and [Fe/H] data in the ranges 5500 K $< T_{\rm eff} <$ 6720 K, log $g \gtrsim 3.5$, and [Fe/H] < -1.5. As well as $T_{\rm eff}$, log g, and [Fe/H] we catalogued A(Li) and/or equivalent widths of the Li I doublet. We excluded CEMP-s stars given that their carbon and lithium abundances have been modified as the result of binary stellar evolution effects, together with CEMP-r/s stars.[6]

As will be discussed in more detail below, A(Li) values depend significantly on the different methods adopted by authors to determine $T_{\rm eff}$ values. We chose data samples to be as large as possible with a view to determining systemic differences between the effective temperatures of the various sources. This initially resulted in 11 data subsets, each from an individual paper or from multiple papers by closely related co-workers. In all but one case, we accepted results based on observations original to the authors. In an approximate time sequence, the 11 subsets (and their numbers of stars) are: Thorburn (1994; 76 stars), Ryan et al. (1999, 2001a, b; 31), Fulbright (2000; 20), Ford et al. (2002; 10), Asplund et al. (2006; 18), Aoki and co-workers (Aoki et al. 2009; Aoki, Ito & Tajitsu 2012; Li et al. 2015; Matsuno et al. 2017a, b; 23), Sbordone et al. (2010; 29)[7] Meléndez et al. (2010, and references therein; 62)[8] Bonifacio et al. (2012, 2015, 2018; 25), Roederer et al. (2014; 127), and Reggiani and co-workers (Placco et al. 2016; Reggiani et al. 2017; 24). These sources provide the lithium and iron abundances necessary for our investigation. To the best of our knowledge, all of the values we have used are based on 1D, LTE analyses.

The above exceptional data subset is that of Meléndez et al. (2010), which adopts material from several sources in the literature to produce high-quality IRFM $T_{\rm eff}$ values, which we shall use below to 'correct' the literature $T_{\rm eff}$ values of other sources to the IRFM scale.

These 11 subsets were augmented by a twelfth that comprises 14 'miscellaneous' near-main-sequence stars, with $-6.0 <$ [Fe/H] < -2.8. Five of these have detected carbon abundances in the range $2.6 <$ [C/Fe] < 4.2, while a further six have limits between [C/Fe] < 1.3 and [C/Fe] < 2.0. The sources of these data are Hansen et al. (2015), Frebel et al. (2008, 2019), Spite et al. (2013), Aguado et al. (2019), Caffau et al. (2012, 2016), Starkenburg et al. (2018), and Lardo et al. (2021).

3 CORRECTING THE AVAILABLE $T_{\rm EFF}$, [FE/H], AND A(LI) VALUES

We examined the data for these stars in three ways. First, we adopted the basic data from the literature; secondly, we transformed the $T_{\rm eff}$, [Fe/H], and A(Li) literature values onto the IRFM $T_{\rm eff}$ scale by using the $T_{\rm IRFM}$ based values of Meléndez et al. (2010); and thirdly, we determined IRFM $T_{\rm eff}$ values *ab initio* based on broad-band infrared colours, complemented by $(g - i)$ observations, as available.

3.1 Step 1 – The literature data

Fig. 2 presents the dependence of A(Li) as a function of $T_{\rm eff}$ and [Fe/H] for the 12 data sets for stars initially chosen to have $T_{\rm eff} >$ 5500 K and [Fe/H] < -1.50. In what follows, we shall refer to this as the 'Literature' sample. Also shown in the figure is the slope of the linear line of best fit in the (A(Li), [Fe/H]) – plane in the range $-3.5 \lesssim$ [Fe/H] $\lesssim -1.5$ – which has been discussed at some length by several workers (e.g. Thorburn 1994; Ryan et al. 1999), together with the RMS dispersion of the data points about the lines of best fit (excluding stars with only limiting values).[9] Setting aside the subset of 'miscellaneous' stars having [Fe/H] < -2.8 (in the bottom-right

[4]Carbon-Enhanced-Metal-Poor (C-rich) stars with [C/Fe] > 0.7 and [Ba/Fe] < 0.0 (Beers & Christlieb 2005; Aoki et al. 2007).

[5]We draw the reader's attention to the fact that in Table 1, we identified several other potential causes of observed lithium abundances below the Spite Plateau – in particular basic stellar evolutionary effects, e.g. diffusion (Deliyannis et al. 1990); turbulent mixing within the stars themselves (Richard et al. 2005); and universal destruction of lithium by a first generation of stars following the Big Bang (Piau et al. 2006). Our only justification for this is that they are not necessary in the suggestions we shall make.

[6]See Beers & Christlieb (2005), Lucatello et al. (2005), and Aoki et al. (2007) for details concerning these stars.

[7]Throughout the present work, we adopt the $A(Li)_{1D,\,LTE}$, IRFM-based results in table 4 of Sbordone et al. (2010), in preference to the results therein based on other methods.

[8]We utilize the $A(Li)_{1D,\,LTE}$ values in table 1 of Meléndez et al. (2010).

[9]We note for completeness that we have excluded the 3σ outlier (CS 22188-033) when determining the line of best fit for the Sbordone et al. (2010) data.

Downloaded from https://academic.oup.com/mnras/article/522/1/1358/7095871 by guest on 27 April 2025

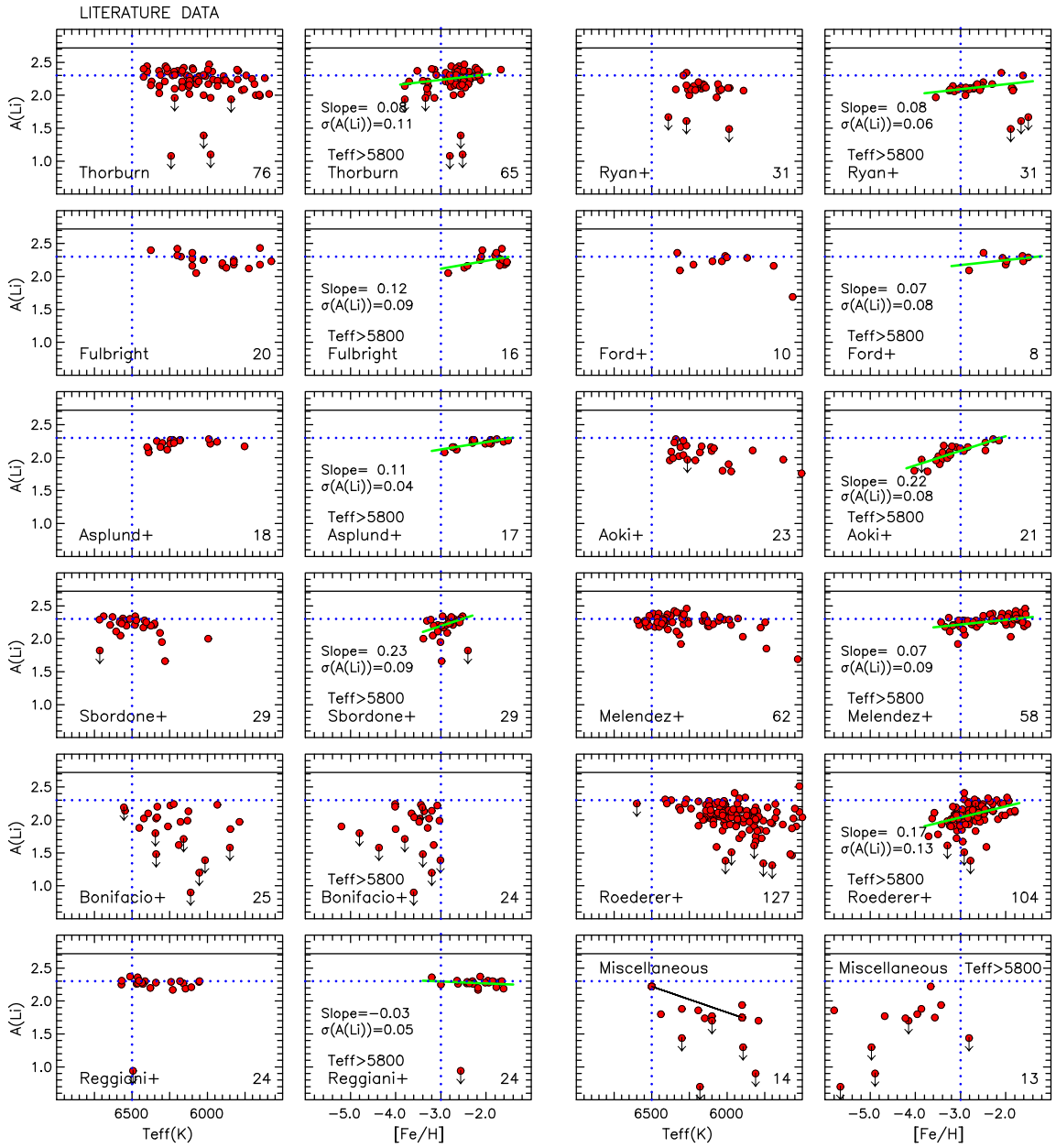

Figure 2. A(Li) versus $T_{\rm eff}$ and [Fe/H] for the 12 'Literature' data samples. The black horizontal lines represent Primordial Lithium $(A(Li)_P = 2.72)$. The legends within each panel identify the sample and (at bottom-right) the number of points in the panel. In panels with [Fe/H] abscissae, the sloping line of best fit is shown (where appropriate) for stars in the range $-3.5 \lesssim$ [Fe/H] $\lesssim -1.5$, for which the slope and RMS scatter are also presented; the adopted $T_{\rm eff}$ lower limit is included. The co-joined points represent the EMP double-lined spectroscopic binary CS 22876-032. The dotted blue lines are the same in all panels and included to facilitate comparison between the data sets. See text for discussion.

panel of the figure), we comment on two basic aspects of the other 11 data sets.

3.1.1 Systemic differences between literature values

Perhaps the most important differences in Fig. 2 are those caused by systemic $T_{\rm eff}$ differences. In particular, the hotter stars of Thorburn (1994), Ryan et al. (1999, 2001a, b), Fulbright (2000), Ford et al. (2002), Asplund et al. (2006), Aoki and co-workers (Aoki et al. 2009; Aoki et al. 2012; Li et al. 2015; Matsuno et al. 2017a, b), and Roederer et al. (2014) are some 200–350 K cooler than those of Sbordone et al. (2010) and Meléndez et al. (2010), both of which have IRFM-based $T_{\rm eff}$. This is driven, in very large part, by significant differences in the assumptions and methods with which the temperatures have been derived. We shall address this issue in Section 3.2.

We remind the reader that, fortuitously, $A(Li)_{1D,\,LTE}$ abundances differ only slightly from the more realistic $A(Li)_{3D,\,NLTE}$ values, with $A(Li)_{3D,\,NLTE} - A(Li)_{1D,\,LTE} \sim 0.05$, as first reported by Asplund et al. (2003) and Asplund (2005).

3.1.2 What is the lower T_{eff} *limit of the Spite Plateau?*

As noted by Spite & Spite (1982), the plateau effect in the A(Li) versus $T_{\rm eff}$ plane falls away at lower temperatures as a result of

Downloaded from https://academic.oup.com/mnras/article/522/1/1358/7095871 by guest on 27 April 2025

the increasing depth of the surface convective zone, which leads to lithium destruction by proton fusion. The data of their tables 3 and 5 define the Spite Plateau to lie within the ranges 5500 K $< T_{\rm eff} <$ 6250 K and $-2.4 <$ [Fe/H] < -1.1 (for objects on their $T_{\rm eff}$ and [Fe/H] scales). In the A(Li) versus $T_{\rm eff}$ panels in Fig. 2 we have therefore chosen to plot stars with $T_{\rm eff} > 5500$ K. It is clear, however, that in some half of the data sets in Fig. 2 $T_{\rm eff} = 5800$ K would be a safer estimate of the limit (presumably as the result of different $T_{\rm eff}$ scales). Accordingly, in the A(Li) versus [Fe/H] panels in Fig. 2 we have plotted only stars with $T_{\rm eff} > 5800$ K.

Meléndez et al. (2010, see their fig. 2) report that the lower $T_{\rm eff}$ limit of the plateau is a function of [Fe/H], increasing as [Fe/H] decreases. The effect is evident in the Melendez et al. panel in our Fig. 2 which is suggestive of a limit of $T_{\rm eff} = 6000$ K. Further support for the concept is suggested by the components of the extremely metal-poor (EMP), double-lined, spectroscopic binary CS 22876-032, which have $T_{\rm eff} = 6500$ K and 5900 K, [Fe/H] $= -3.66$ and -3.57, and the very different lithium abundances A(Li) = 2.22 and 1.75, respectively (González Hernández et al. 2008). This effect can be seen in the bottom right-most (A(Li), $T_{\rm eff}$) panels of our Figs 2 (and 4), where the two stars are co-joined. The simplest explanation of the large difference in lithium abundance of ΔA(Li) = 0.47 in this system is that not only does the effective temperature of the cooler secondary star lie below that of the cool edge of the Spite Plateau but also that the cool edge of the plateau may have moved to even higher temperature for abundances below [Fe/H] $= -3.6$.

3.2 Step 2 – 'Corrected' effective temperatures on the IRFM scale

A(Li) is sensitive to the differences in $T_{\rm eff}$ resulting from the several methods adopted in the literature. As noted above, systemic differences in the manner in which literature $T_{\rm eff}$ values are determined cause differences of order 200–350 K. An error of 300 K results in the lithium abundance changing by ΔA(Li) ~ 0.25 dex. To address this issue, we sought to 'correct' all literature $T_{\rm eff}$ values to the IRFM scale by adopting the IRFM $T_{\rm eff}$ values of Meléndez et al. (2010) as standards, and which we shall refer to as 'Corrected-Literature' values. We regard the IRFM method adopted by Melendez et al. (2010), in particular the use of interstellar Na D lines to determine $E(B-V)$ values, as a positive step forward.

Fig. 3 and Table 2 quantify the mean differences of $\Delta T_{\rm eff} = T_{\rm eff}$(Author) – $T_{\rm eff}$(Melendez) versus $T_{\rm eff}$(Melendez), Δ[Fe/H] = [Fe/H](Author) – [Fe/H](Melendez) versus [Fe/H](Melendez), and ΔA(Li) = A(Li)(Author) – A(Li)(Melendez) versus A(Li)(Melendez) for the nine literature subsets that have a sufficient overlap of stars with those of Meléndez et al. (2010). These differences are driven essentially by those in $T_{\rm eff}$ between the literature temperature scales and the IRFM scale adopted by Meléndez et al. (2010) and bring the literature values onto the IRFM scale. Columns (1) and (2) of the table contain the authorship and methods used to determine $T_{\rm eff}$, while columns (3)–(6) present the resulting $\langle\Delta T_{\rm eff}\rangle$, $\langle\Delta$[Fe/H]$\rangle$, $\langle\Delta$A(Li)$\rangle$, and number of stars, respectively.

The two literature subsets that do not have sufficient overlap with Meléndez et al. (2010) are those of Bonifacio et al. (2012, 2015, 2018) and the twelfth subset of 14 miscellaneous stars having [Fe/H] < -2.8 (occupying the bottom-right panels of Fig. 2). In Section 3.3, we shall discuss IRFM corrections to the literature values of $T_{\rm eff}$, [Fe/H], and A(Li) of the Bonifacio et al. data, which we have also included in Table 2. For the 'miscellaneous' subset, we have applied no correction.

Fig. 4 which has the same format as Fig. 2 presents the 'Corrected' results when the differences in Table 2 (including those of Bonifacio et al.) are applied to the literature $T_{\rm eff}$, [Fe/H], and A(Li) values. In Fig. 2 we applied an exclusion of stars having $T_{\rm eff} < 5800$ K from the (A(Li), [Fe/H]) – plane. In view of the corrections that have been made to the literature $T_{\rm eff}$ values, which are of order +200 K, we have adopted $T_{\rm eff} < 6000$ K as being at or above the cooler limit of the Spite Plateau in the (A(Li), [Fe/H]) – plane of Fig. 4. The slopes and RMS dispersions of the data about the linear lines of best fit in the (A(Li), [Fe/H]) – planes (introduced in Fig. 2) are presented in Fig. 4 and in columns (7) and (8) of Table 2.

A comparison between Figs 2 and 4 reveals the following: (1) there is better agreement in Fig. 4 between the effective temperatures of the hotter stars of a majority of the panels; (2) there are subtle improvements in A(Li) values bringing them closer to a common plateau; (3) a large dispersion of σ(A(Li)) = 0.14 remains in the Roederer et al. (2014) sample, which is not too surprising insofar as they estimate that the error in their Li abundances is $\sim$0.10–0.20 dex; and (4) the Bonifacio et al. data, which have [Fe/H] < -3.0, stretch to lower [Fe/H] than the other samples and show large scatter. This dispersion is the Sbordone et al. and Bonifacio et al. 'meltdown'.

Given the larger size of the Roederer et al. (2014) errors relative to those of the other samples, we choose not to include this data set further in our discussions of lithium abundances.

Table 3 presents the 'Literature' and 'Corrected-Literature' of 332 literature observations of the 195 individual stars in the data sets presented in Figs 2 and 4 (excluding the Roederer et al. 2014 data). Column (1) contains the star number, columns (2) and (3) contain the star name and coordinates, columns (4)–(7) present $T_{\rm eff}$, log g, [Fe/H], and A(Li) for the 'Literature' data set, columns (8)–(10) have $T_{\rm eff}$, [Fe/H], and A(Li) for the 'Corrected-Literature' sample, and column (11) shows code for the original data sources.

3.3 Step 3 - *ab initio* temperatures on the IRFM scale

To complement the two previous steps, we analysed the literature equivalent widths of the Li I 6707 Å doublet[10] together with independent *ab initio* IRFM $T_{\rm eff}$ values based on visual and infrared colours, using the algorithm of Sbordone et al. (2010, table B.1) to determine A(Li)$_{\rm 1D,\,LTE}$ values. This procedure also requires input [Fe/H] values, to which it is relatively insensitive,[11] and for which we adopted the 'corrected' [Fe/H] values of Step 2. We used literature log g values (or log $g = 4.0$ in their absence), to which the process is insensitive for near-main-sequence stars.

In order to determine IRFM $T_{\rm eff}$ (hereafter $T_{\rm IRFM}$) from visual and infrared observations ($V-I$, $V-J$, and $V-K$ data), we adopted photometric data from the Simbad archives, and UCAC4 (Zacharias et al. 2013) and APASS (Henden et al. 2016) values from the VizieR archives.[12] Reddening estimates followed Meléndez et al. (2006, section 4.1)[13] and we accepted stars having $E(B-V) \leq 0.10$ and Galactic latitude |b| > 30. All reddenings determined in the present

[10]For the some 40 stars in the literature data that have A(Li) but no published equivalent widths, we used the Sbordone et al. (2010, table B.1) algorithm, together with literature A(Li), $T_{\rm eff}$, [Fe/H], and log g to obtain those values.
[11]By way of example, at $T_{\rm IRFM} = 6000$ K, a change of Δ[Fe/H] of 0.5 dex causes a change in $T_{\rm IRFM}$ of order 20–50 K.
[12]https://simbad.unistra.fr/simbad/ and https://vizier.u-strasbg.fr. Magnitudes were accepted only if errors were less than 0.03 for V, I, J, and K and 0.05 for g and i.
[13]We are grateful to J. Melendez for making available the Fortran code 'extinct.for' of Hakkila et al. (1997),

Downloaded from https://academic.oup.com/mnras/article/522/1/1358/7095871 by guest on 27 April 2025

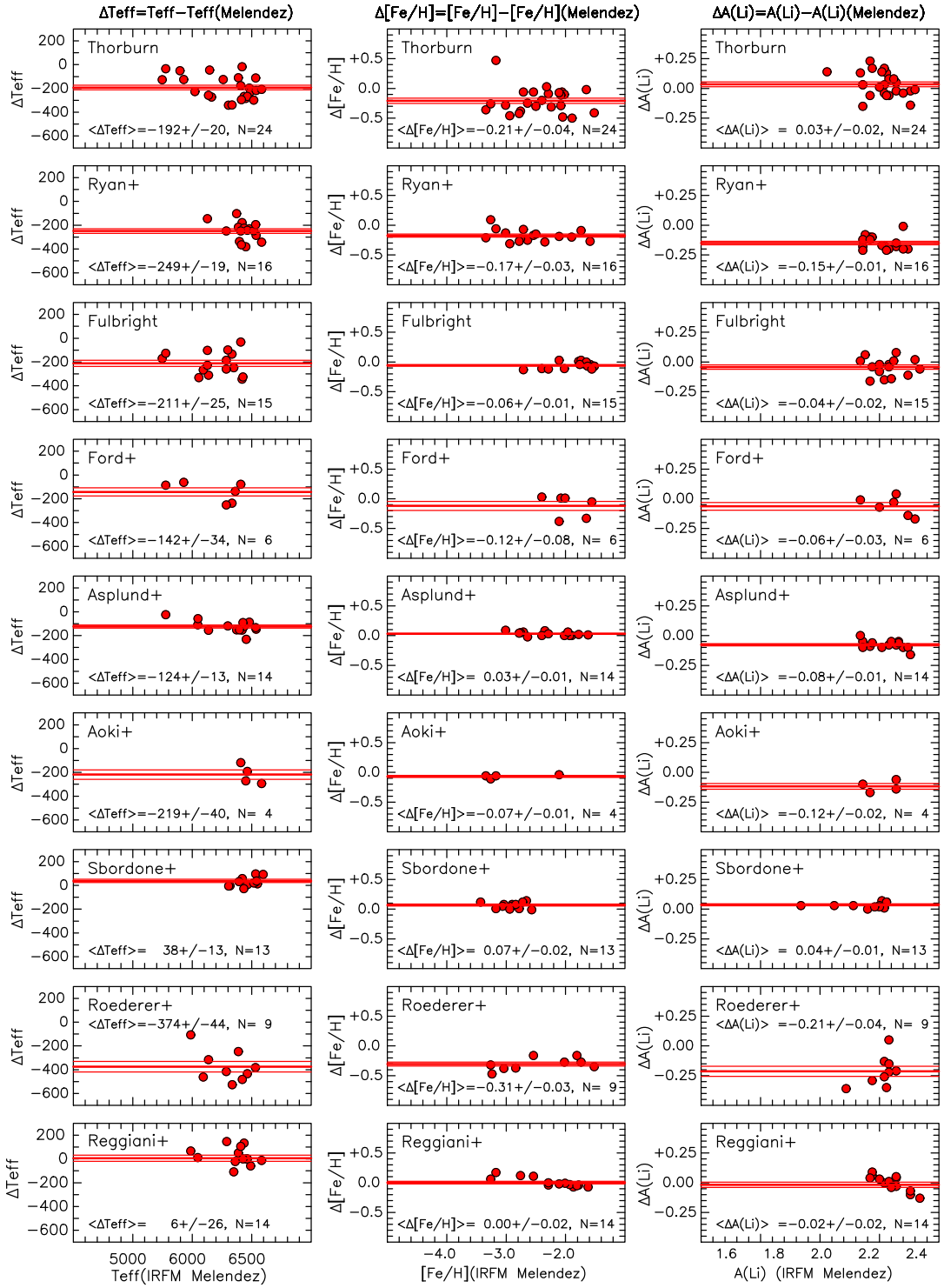

Figure 3. Δ $T_{\rm eff}$ versus $T_{\rm eff}$ (IRFM Melendez), Δ[Fe/H] versus [Fe/H] (IRFM Melendez) and ΔA(Li) versus A(Li) (IRFM Melendez) for nine data subsets. The authors, mean differences with errors, and number of data points appear within each panel.

paper have utilized this procedure, using distances obtained from the Gaia EDR3 archive (https://gea.esac.esa.int/archive/); see also Gaia Collaboration (2016 and 2021) and the IRFM ($T_{\rm eff}$, colour) fits of Casagrande et al. (2010).

As foreshadowed above for the Bonicacio et al. stars, which do not have sufficient overlap with the Meléndez et al. (2010) subset, we proceeded as follows. Using stars in our sample that have both $T_{\rm IRFM}$ and APASS ($g-i$) values, we determined the linear least-squares fit to $T_{\rm IRFM}$ versus $(g-i)_0$: $T_{\rm IRFM}((g-i)_0) = 6756.4 - 959.7(g-i)_0$ (K) (34 stars, yielding RMS = 182 K). The fit to the data is presented in Fig. 5. We then used the SDSS ($g-i$) values from Bonifacio et al. (2012, 2015, 2018) to obtain temperatures using this relationship. It is of interest to compare our $T_{\rm IRFM}((g-i)_0)$ values with the infrared temperatures of Bonifacio et al. While their $T_{\rm eff}$ values were based

Downloaded from https://academic.oup.com/mnras/article/522/1/1358/7095871 by guest on 27 April 2025

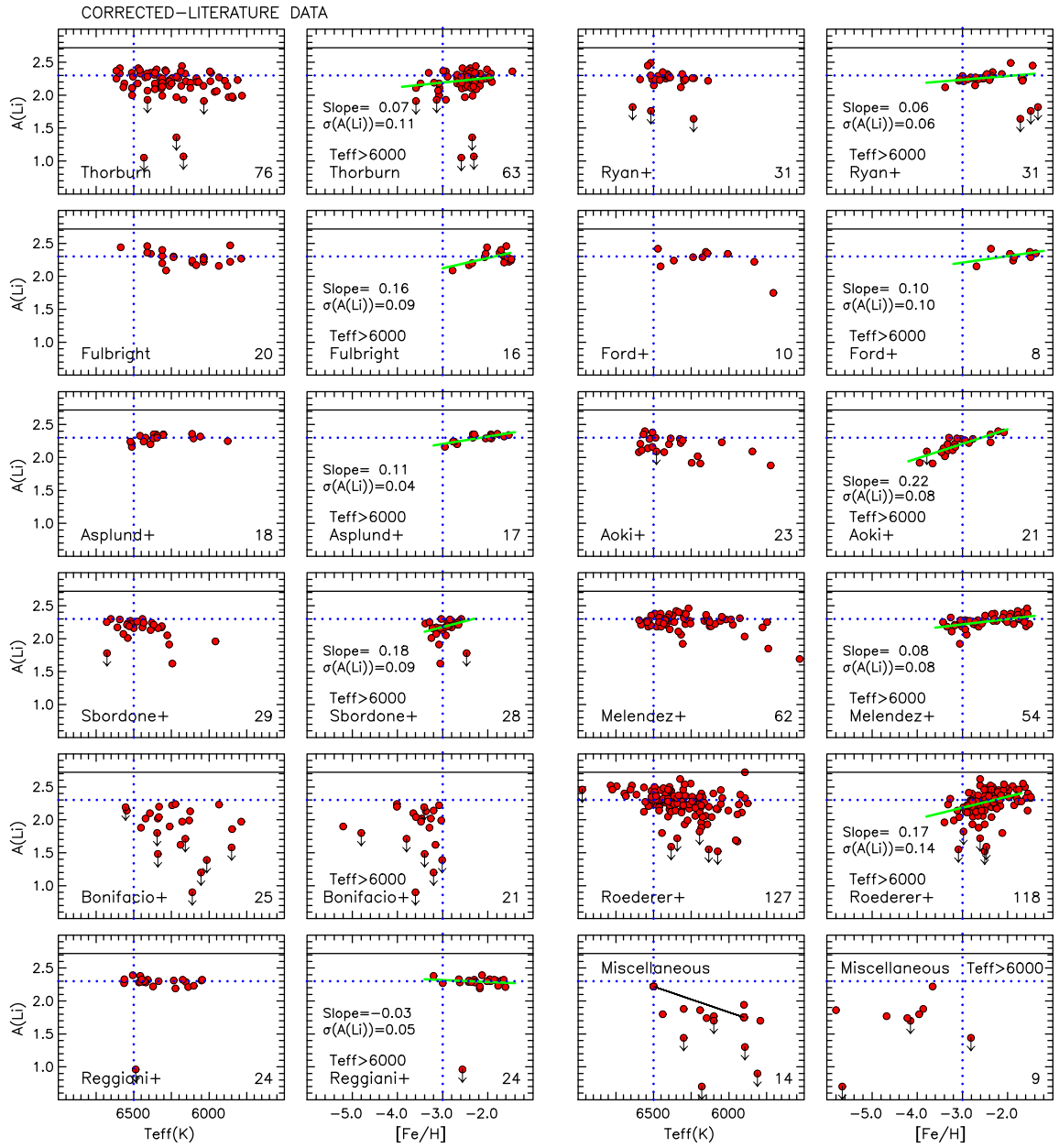

Figure 4. A(Li) versus $T_{\rm eff}$ and [Fe/H] for the 12 data samples, when the 'Literature' values have been 'Corrected' to the IRFM temperature scale of Meléndez et al. (2010). The format is the same as that of Fig. 2. See text for discussion.

on SDSS $(g - z)$ colours, ours utilize SDSS $(g - i)$. From 25 stars in common, we find a mean difference $\langle \Delta\ T_{\rm eff} \rangle = \langle\ T_{\rm eff}$(Bonifacio et al.) – $T_{\rm IRFM}((g - i)_0) \rangle = -204 \pm 21$ K. We adopt this result to determine IRFM corrections to the Bonifacio et al. literature values in Table 2: $\Delta\ T_{\rm eff} = -204$ K, Δ[Fe/H] $= -0.20$ (*cf.* Yong et al. 2013a) and ΔA(Li) $= -0.16$, [utilizing the Sbordone et al. (2010, table B.1) algorithm].

Table 4 presents the averaged data for the 195 individual stars. Columns (1) and (2) contain star name and coordinates, columns (3)–(5) present $T_{\rm eff}$, [Fe/H], and A(Li) for the 'Literature' data set, and columns (6)–(8) have the same parameters for the 'Corrected-Literature' sample, respectively. Column (9) contains the number of data sources included in the average for each star, while columns (10)–(12) list $T_{\rm eff}$, [Fe/H], and A(Li) values for 121 stars from the '*ab initio* IRFM' step.

3.4 Comparison of the three data steps

At this point, we have up to three independent A(Li) values for each of the 195 individual stars. Fig. 6 presents the dependence of A(Li) versus $T_{\rm eff}$ as a function of [Fe/H] for the above three steps, where rows (a)–(c) contain the 'Literature', 'Corrected-Literature', and, '*ab initio* IRFM' results, respectively. In each row of the figure, there are five panels containing (A(Li), $T_{\rm eff}$) values for stars in the [Fe/H] range indicated within each panel. Note that the [Fe/H] ranges are the same in each column of the figure. In all panels, the blue horizontal dotted line represents A(Li) = 2.3, which is useful to facilitate comparison of the results. At the bottom left of each panel, the three numbers represent the mean A(Li), its dispersion σ(A(Li)), and the number of stars. For completeness, in Fig. 7 we show the complementary A(Li) versus [Fe/H] diagrams for the three cases.

Downloaded from https://academic.oup.com/mnras/article/522/1/1358/7095871 by guest on 27 April 2025

Table 2. Mean differences relative to Meléndez et al. (2010) and A(Li) versus [Fe/H] slopes.

Authors	$T_{\rm eff}$ Source	$\langle\Delta T_{\rm eff}\rangle$ [1]	$\langle\Delta$[Fe/H]$\rangle$ [2]	$\langle\Delta$A(Li)$\rangle$ [3]	N[4]	Slope[5]	RMS[6]	N[4]
(1)	(2)	(3)	(4)	(5)	(6)	(7)	(8)	(9)
Thorburn (1994)	Colours	−192	−0.21	0.03	24	0.07	0.11	58
Ryan et al.[7]	Colours & H lines	−249	−0.17	−0.15	16	0.06	0.06	27
Fulbright (2000)	EPM[8]	−211	−0.06	−0.04	15	0.16	0.09	14
Ford et al. (2002)	IRFM	−142	−0.12	−0.06	6	0.10	0.10	6
Asplund et al. (2006)	Hα line	−124	0.03	−0.08	14	0.11	0.04	17
Aoki et al.[9]	H lines & colours	−219	−0.07	−0.12	4	0.22	0.08	19
Sbordone et al. (2010)	IRFM	38	0.07	0.04	13	0.18	0.09	26
Melendez et al. (2010)	IRFM	...	...	...	...	0.08	0.08	54
Bonifacio et al.[10]	Colours	−204	−0.20	−0.16	25	...	...	..
Roederer et al. (2014)	EPM[8]	−374	−0.31	−0.21	9	0.17	0.14	110
Reggiani et al.[11]	DEPM[12]	6	0.00	−0.02	14	−0.03	0.05	23

Notes. [1] $\Delta T_{\rm eff} = T_{\rm eff}$(Author) – $T_{\rm eff}$(Melendez); [2] Δ[Fe/H] = [Fe/H](Author) – [Fe/H](Melendez); [3] ΔA(Li) = A(Li)(Author) – A(Li)(Melendez); [4]Number of stars; [5]Slope of linear fit in Fig. 4; [6]RMS about linear fit in Fig. 4; [7]Ryan et al. (1999, 2001b),[8]Excitation Potential Method,[9]Aoki et al. (2009, 2012), Matsuno et al. (2017a, b), Li et al. (2015); [10]Bonifacio et al. (2012, 2015, 2018; see Section 3.3); [11]Placco et al. (2016), Reggiani et al. (2017); [12]Differential Excitation Potential Method.

Table 3. Multiple observations of 'Literature' and 'Corrected-Literature' data.

Star No.	Starname	Coordinates (2000)	$T_{\rm eff}$ (Lit)	log g (Lit)	[Fe/H] (Lit)	A(Li) (Lit	$T_{\rm eff}$ (Corr)	[Fe/H] (Corr)	A(Li) (Corr)	Author[1]
(1)	(2)	(3)	(4)	(5)	(6)	(7)	(8)	(9)	(10)	(11)
1	CS 22876-032A	00 07 37.10 − 35 31 15.0	6319	4.00	−3.80	2.14	6511	−3.59	2.11	TH94
	CS 22876-032A	00 07 37.10 − 35 31 15.0	6500	4.40	−3.66	2.22	6500	−3.66	2.22	GO08
2	CS 22876-032B	00 07 37.10 − 35 31 15.0	5900	4.60	−3.57	1.75	5900	−3.57	1.75	GO08
3	LP 824-188	00 11 17.63 − 20 43 30.7	5890	4.00	−1.84	2.07	6139	−1.67	2.22	RY99
4	BS 17570-063	00 20 36.19 + 23 47 37.6	6315	4.70	−2.86	2.09	6277	−2.93	2.05	SB10
	BS 17570-063	00 20 36.19 + 23 47 37.6	6318	4.69	−2.91	2.06	6318	−2.91	2.06	ME10
5	SD 0021–0050	00 21 13.78 − 00 50 05.2	6546	4.30	−3.20	2.14	6750	−3.00	2.30	BO12
6	SD 0023 + 0307	00 23 14.00 + 03 07 58.1	6192	4.70	<-5.80	1.86	6192	<-5.80	1.86	AGFR
7	SD 0027 + 1404	00 27 49.46 + 14 04 18.1	6125	3.61	−3.37	2.13	6329	−3.17	2.29	BO12
8	CS 29527-015	00 29 10.68 − 19 10 07.3	6578	4.50	−3.31	2.27	6540	−3.38	2.23	SB10
	CS 29527-015	00 29 10.68 − 19 10 07.3	6541	4.24	−3.43	2.25	6541	−3.43	2.25	ME10
9	CS 30339-069	00 30 16.00 − 35 56 55.0	6375	4.40	−2.98	2.20	6337	−3.05	2.16	SB10
10	CS 22882-027	00 38 09.80 − 31 47 58.0	6714	4.70	−2.40	<1.82	6676	−2.47	<1.78	SB10
11	CD −33 239	00 39 51.92 − 33 03 14.1	5993	4.00	−1.87	2.11	6242	−1.70	2.26	RY99
12	SD 0040 + 1604	00 40 29.17 + 16 04 16.2	6360	4.40	−3.29	1.99	6579	−3.22	2.11	AO09
	SD 0040 + 1604	00 40 29.17 + 16 04 16.2	6422	3.90	−3.26	2.02	6626	−3.06	2.18	BO12
13	BD + 71 31	00 43 44.34 + 72 10 43.1	6156	4.00	−2.23	2.42	6348	−2.02	2.39	TH94
14	CS 22188-033	00 51 26.17 − 38 12 17.8	6281	4.50	−2.98	1.66	6243	−3.05	1.62	SB10
15	CS 29514-007	01 06 40.50 − 24 58 41.0	6351	4.30	−2.79	2.23	6313	−2.86	2.19	SB10
16	CS 29518-020	01 12 13.21 − 31 00 05.3	6471	4.90	−2.60	2.28	6433	−2.67	2.24	SB10
	CS 29518-020	01 12 13.21 − 31 00 05.3	6464	4.67	−2.72	2.25	6464	−2.72	2.25	ME10
17	CS 29518-043	01 18 38.30 − 30 41 02.8	6537	4.25	−3.16	2.20	6499	−3.23	2.16	SB10
	CS 29518-043	01 18 38.30 − 30 41 02.8	6517	4.28	−3.17	2.20	6517	−3.17	2.20	ME10
18	SD 0120–1001	01 20 32.63 − 10 01 06.5	5627	3.40	−3.84	1.97	5846	−3.77	2.09	MA17
19	CS 22953-037	01 25 06.80 − 59 15 57.0	6557	4.45	−2.76	2.28	6519	−2.83	2.24	SB10
	CS 22953-037	01 25 06.80 − 59 15 57.0	6532	4.33	−2.84	2.27	6532	−2.84	2.27	ME10
20	SD 0140 + 2344	01 40 36.22 + 23 44 58.0	5848	4.00	−4.00	1.86	6052	−3.80	2.02	BO18
21	BD + 02 263	01 45 13.81 + 03 30 49.2	5800	4.00	−2.35	2.24	5992	−2.14	2.21	TH94
22	G 245-32	01 47 12.38 + 73 28 27.1	6290	4.00	−1.62	2.30	6539	−1.45	2.45	RY99
23	BD −10 388	01 50 32.64 − 09 21 02.8	6135	4.00	−2.29	2.30	6327	−2.08	2.27	TH94
	G 271-162	01 50 32.64 − 09 21 02.8	6230	3.93	−2.30	2.27	6354	−2.33	2.35	AS06
	BD −10 388	01 50 32.64 − 09 21 02.8	6260	3.98	−2.32	2.27	6260	−2.32	2.27	ME10

Notes. [1]Author: AGFR = (Aguado et al. 2019; Frebel et al. 2019), AO09 = Aoki et al. (2009), AO12 = Aoki et al. (2012), AS06 = Asplund et al. (2006), BO12 = Bonifacio et al. (2012), BO15 = Bonifacio et al. (2015), BO18 = Bonifacio et al. (2018), CA12 = Caffau et al. (2012), CA16 = Caffau et al. (2016), FO02 = Ford et al. (2002), FR08 = Frebel et al. (2008), FU00 = Fulbright (2000), GO08 = González Hernández et al. (2008), HA15 = Hansen et al. (2015), LA21 = Lardo et al. (2021), LI15 = Li et al. (2015), MA17 = (Matsuno et al. 2017a, b), ME10 = Meléndez et al. (2010), RE17 = (Placco et al. 2016; Reggiani et al. 2017), RY99 = (Ryan et al. 1999; Ryan et al. 2001b), SB10 = Sbordone et al. (2010). SP13 = Spite et al. (2013), ST18 = Starkenburg et al. (2018), TH94 = (Thorburn 1994).
This table is published in its entirety in the electronic edition of the paper. A portion is shown here for guidance regarding its form and content.

Downloaded from https://academic.oup.com/mnras/article/522/1/1358/7095871 by guest on 27 April 2025

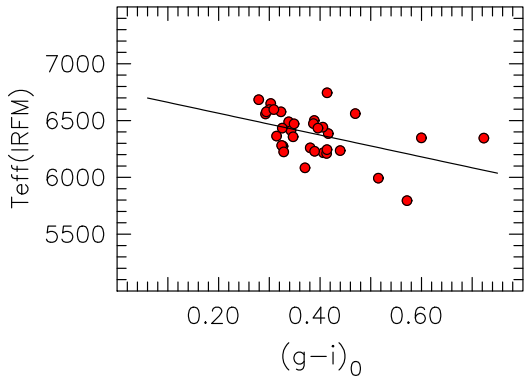

Figure 5. $T_{\rm IRFM}$ versus $(g - i)_0$: $T_{\rm IRFM}((g - i)_0) = 6756.4 - 959.7(g - i)_0$ (K) (34 stars, yielding RMS = 182 K).

While the three rows in Fig. 6 show slight differences, there are clear similarities. Here, we shall discuss our conclusions with reference to the 'Corrected-Literature' middle row, which we regard as the most reliable of the three. Recalling that the A(Li) versus $T_{\rm eff}$ format was the one first used by Spite & Spite (1982) to define what became known as the Spite Plateau, we make the following points: (1) in the right-most panel, which covers $-2.2 <$ [Fe/H] < -1.5, the lithium abundances are constant for $T_{\rm eff} > 6000$ K, as reported by Spite & Spite (1982); then (2) as one proceeds from higher to lower [Fe/H] values in the figure, ⟨A(Li)⟩ decreases; while (3) the dispersion σ(A(Li)) increases. In the bottom of each panel, the three numbers are ⟨A(Li)⟩, σ(A(Li)), and number of stars, respectively. These data are also presented, together with ⟨[Fe/H]⟩, in Table 5, and plotted in Fig. 8 where the left column contains the dependence of ⟨A(Li)⟩ on ⟨[Fe/H]⟩ and the right presents the dispersion, σ(A(Li)) versus ⟨[Fe/H]⟩.

3.4.1 Colour–Magnitude Diagrams (CMDs) for the three data steps

A byproduct of the present investigation is that given $T_{\rm eff}$, V magnitudes, and distances, one is able to construct (M_V, $T_{\rm eff}$) – colour–magnitude diagrams (CMDs), and to compare them with theoretical isochrones in an effort to test the $T_{\rm eff}$ values determined above. In Fig. 9 we present M_V versus $T_{\rm eff}$ CMDs for the three $T_{\rm eff}$ cases discussed above, where each of the three groupings in the figure contains four subpanels embracing different [Fe/H] ranges, together with the Yale-Yonsei isochrones of Demarque et al. (2004)[14], adopting an age of 12 Gyr, for the ranges presented in the subpanels. Inspection of the middle panel, which contains the 'Corrected-Literature' results, offers strong and reassuring support for the procedures we have adopted in Section 3.2.

4 CARBON ABUNDANCES, [C/FE], IN THE RANGE −6.0 < [FE/H] < −2.0

We noted in our Table 1 that Matsuno et al. (2017b) found no apparent anticorrelation between lithium and carbon at [Fe/H] ~ -3.0 – specifically, they reported the existence of two C-rich (CEMP-no) stars 'near the plateau' with lithium abundances A(Li) = 2.17 and 2.14. Jacobson & Frebel (2015) and Placco et al. (2016) had previously presented similar carbon abundances for three CEMP-no stars that have A(Li) values in the range 1.99 – 2.36. For completeness, the [Fe/H], [C/Fe], [Ba/Fe], and A(Li) values for these five stars are presented in Table 6.

As discussed above, it is well established that the large majority of stars with [Fe/H] < -4.5 are C-rich, and that the majority of those near the main-sequence are also Li-poor. We now investigate to what extent, if any, that relationship exists also in the range $-4.2 <$ [Fe/H] ≤ -2.0. That is to say, is there any connection between A(Li) and [C/Fe] in or near the 'meltdown' zone?

[C/Fe] values from the literature are presented for 78 near-main-sequence stars having [Fe/H] ≤ -2.0 in Table 7.[15] The data derive principally from the subsets discussed in Section 3: Frebel et al. (2008, 2019), Bonifacio et al. (2009, 2012, 2018), Caffau et al. (2011, 2012, 2016), Spite et al. (2013), Hansen et al. (2015), Jacobson & Frebel (2015), Li et al. (2015), Placco et al. (2016), Matsuno et al. (2017a, b), Starkenburg et al. (2018), Aguado et al. (2019), and Lardo et al. (2021), and are supplemented by material from Tomkin et al. (1992), Honda et al. (2004), Barklem et al. (2005), Sivarani et al. (2006), Lai et al. (2008), Alexeeva & Mashonkina (2015), Norris & Yong (2019), and Matas Pinto et al. (2021). Fig. 10 presents [C/Fe] versus A(Li) for three [Fe/H] ranges, for stars having $T_{\rm eff} > 6000$ K: (a) [Fe/H] < -4.5 (the most-Fe-poor observed stars), (b) $-4.2 <$ [Fe/H] ≤ -3.0 (the 'meltdown' region), and (c) $-3.0 <$ [Fe/H] ≤ -2.0 (our upper [Fe/H] region).

As part of our investigation, we sought to confirm the [C/Fe] abundances of four stars in Table 7 that have both low A(Li) and low [C/Fe] and for which spectra are available in the ESO UVES archives, using the techniques adopted in Norris & Yong (2019). These are CS 22882-027 with (A(Li), [C/Fe]) = (<1.78, <0.24), CS 22188-033 (1.62, <0.84), BS 17570-063 (2.05, 0.49), and CS 22966-011 (1.91, 0.54). Our results were essentially the same as reported by the authors (Bonifacio et al. 2009 and Matas Pinto et al. 2021) in Table 7, except that for BS 17570-063 and CS 22966-011 we obtained abundances that we regarded as limits rather than detections.

Defining C-rich stars as those with [C/Fe] > 0.7 (following Aoki et al. 2007), one finds that the most metal-poor regime ([Fe/H] < -4.5) in Table 7 has an extremely high C-rich fraction of 1.00, as might be expected from our previous discussion. The potentially more significant and important result in the present context, however, appears in the 'meltdown' regime ($-4.2 <$ [Fe/H] ≤ -3.0), where the incidence of stars with [C/Fe] > 0.7 is very high. That is, the fraction of stars with detected carbon and [C/Fe] > 0.7 is 0.52. If any of the stars with a limit above [C/Fe] = 0.7 turned out to be C-rich, the C-rich fraction would be greater that 0.52.[16]

Inspection of the data in Table 7 permits us to investigate more closely the stars in the range $-3.0 <$ [Fe/H] < -2.5 that have the smallest [C/Fe] values. Of particular interest for the present discussion are the four stars in Fig. 10 that have [C/Fe] < 0.9 and A(Li) < 1.8, and which offer no support for an anticorrelation of A(Li) and [C/Fe]. They are CS 22882-027 with (A(Li), [C/Fe]) = (<1.78, < 0.24), CS 22188-033 (1.62, < 0.84), HE 0411-3558 (<1.44, < 0.70), and G 186-26 (<1.00, 0.46). Three of these have been identified as belonging to the 'blue-straggler' related group discussed above – the first two by Matas Pinto et al. (2021) and the

[14] http://www.astro.yale.edu/demarque/yyiso.html

[15] We note that the [C/Fe] abundances in Table 7 have been rescaled from the literature values to adopt the [Fe/H] of the table and a solar carbon abundance $A(C)_\odot = 8.43$ (Asplund et al. 2009).

[16] We estimate that for a star with $T_{\rm eff} = 6000$ K, log $g = 4.5$, and [O/Fe] $= +0.4$ to have a detectable CH 4323 Å feature at the 0.98 intensity level relative to the continuum would require [C/Fe] = 1.3.

Downloaded from https://academic.oup.com/mnras/article/522/1/1358/7095871 by guest on 27 April 2025

Table 4. Averaged 'Literature', 'Corrected-Literature', and ' *ab initio* IRFM $T_{\rm eff}$' data.

Starname	Coordinates (2000)	$T_{\rm eff}$ (Lit)	[Fe/H] (Lit)	A(Li) (Lit)	$T_{\rm eff}$ (Corr)	[Fe/H] (Corr)	A(Li) (Corr)	N	$T_{\rm eff}$ (IRFM)	[Fe/H] (IRFM)	A(Li) (IRFM)
(1)	(2)	(3)	(4)	(5)	(6)	(7)	(8)	(9)	(10)	(11)	(12)
CS 22876-032A	00 07 37.10 − 35 31 15.0	6410	− 3.73	2.18	6506	− 3.62	2.16	2	6482	−3.62	2.09
CS 22876-032B	00 07 37.10 − 35 31 15.0	5900	− 3.57	1.75	5900	− 3.57	1.75	1	...	...	...
LP 824-188	00 11 17.63 − 20 43 30.7	5890	− 1.84	2.07	6139	− 1.67	2.22	1	6098	−1.67	2.17
BS 17570-063	00 20 36.19 + 23 47 37.6	6317	− 2.88	2.07	6298	− 2.92	2.05	2	5854	−2.92	1.69
SD 0021–0050	00 21 13.78 − 00 50 05.2	6546	− 3.20	2.14	6750	− 3.00	2.30	1	6549	−3.00	2.14
SD 0023 + 0307	00 23 14.00 + 03 07 58.1	6192	< − 5.80	1.86	6192	< − 5.80	1.86	1	...	...	...
SD 0027 + 1404	00 27 49.46 + 14 04 18.1	6125	− 3.37	2.13	6329	− 3.17	2.29	1	6235	−3.17	2.17
CS 29527-015	00 29 10.68 − 19 10 07.3	6560	− 3.37	2.26	6541	− 3.41	2.24	2	...	...	...
CS 30339-069	00 30 16.00 − 35 56 55.0	6375	− 2.98	2.20	6337	− 3.05	2.16	1	...	...	...
CS 22882-027	00 38 09.80 − 31 47 58.0	6714	− 2.40	<1.82	6676	− 2.47	<1.78	1	...	...	...
CD −33 239	00 39 51.92 − 33 03 14.1	5993	− 1.87	2.11	6242	− 1.70	2.26	1	6413	−1.70	2.37
SD 0040 + 1604	00 40 29.17 + 16 04 16.2	6391	− 3.28	2.01	6603	− 3.14	2.14	2	6275	−3.14	1.90
BD + 71 31	00 43 44.34 + 72 10 43.1	6156	− 2.23	2.42	6348	− 2.02	2.39	1	...	...	...
CS 22188-033	00 51 26.17 − 38 12 17.8	6281	− 2.98	1.66	6243	− 3.05	1.62	1	6365	−3.05	1.72
CS 29514-007	01 06 40.50 − 24 58 41.0	6351	− 2.79	2.23	6313	− 2.86	2.19	1	6357	−2.86	2.22
CS 29518-020	01 12 13.21 − 31 00 05.3	6468	− 2.66	2.26	6449	− 2.70	2.24	2	6501	−2.70	2.27
CS 29518-043	01 18 38.30 − 30 41 02.8	6527	− 3.16	2.20	6508	− 3.20	2.18	2	6576	−3.20	2.22
SD 0120–1001	01 20 32.63 − 10 01 06.5	5627	− 3.84	1.97	5846	− 3.77	2.09	1	...	...	...
CS 22953-037	01 25 06.80 − 59 15 57.0	6545	− 2.80	2.28	6526	− 2.84	2.26	2	6684	−2.84	2.35
SD 0140 + 2344	01 40 36.22 + 23 44 58.0	5848	− 4.00	1.86	6052	− 3.80	2.02	1	5582	−3.80	1.56
BD + 02 263	01 45 13.81 + 03 30 49.2	5800	− 2.35	2.24	5992	− 2.14	2.21	1	6111	−2.14	2.26
G 245-32	01 47 12.38 + 73 28 27.1	6290	− 1.62	2.30	6539	− 1.45	2.45	1	...	...	...
BD −10 388	01 50 32.64 − 09 21 02.8	6208	− 2.30	2.28	6314	− 2.24	2.30	3	6220	−2.24	2.17

Note. This table is published in its entirety in the electronic edition of the paper. A portion is shown here for guidance regarding its form and content.

fourth by Ryan et al. (2001a), suggesting they are not relevant to the question at issue here.

We shall return, in Section 5.5, to our discussion of the 'meltdown', to a possible explanation of the data in Fig. 10.

5 DISCUSSION

Given that the Li abundances in Fig. 6 are strongly dependent on [Fe/H], which to first order increases with time in the early Universe, we are of the view that an explanation of the astration of primordial lithium most likely depends strongly on age and that the lithium profile in the figure results from several unrelated phenomena, which occurred at different places and times over a period of some billion years.

5.1 A comment on the Ryan et al. blue-straggler connection

Against this background, we shall not consider further the 'blue straggler' related lithium-poor stars discussed by Ryan et al. (2001a, 2002). There are relatively few of these objects,[17] and as noted by Bonifacio et al. (2012), the soundness of the blue-straggler hypothesis notwithstanding, their restriction to relatively higher observed values of [Fe/H] suggests they can play only a minor role in our understanding of the complicated lithium abundance patterns at the earliest times. In light of the potential relationship between this class of stars and 'blue stragglers', Ryan et al. (2002) advise, 'such objects must be avoided in studies of the primordial Li abundance and in investigations into the way normal single stars process their initial Li'. One might wonder if near-main-sequence, C-rich, Li-weak stars with [Fe/H] < -3.0 might be rapid rotators. To our knowledge, there exists little information on this possibility. One exception is the analysis of HE 1327–2326 ([Fe/H] $= -5.66$, A(Li) $= <0.70$) by Aoki et al. (2006), who report 'no clear excess (line) broadening by rotation... with respect to Li-normal stars', from their careful high-resolution analysis (R = 60 000).

5.2 Three population II subpopulations

Given the $T_{\rm eff}$ and [Fe/H] of the stars under discussion here, we have implicitly assumed their membership of the Population II that resides in the Galactic halo (see Sandage 1986 and references therein for details of the concept of stellar populations). In what follows, for heuristic purposes, we shall define three Population II subpopulations, which we name Pop IIa, Pop IIb, and Pop IIab. Pop IIa comprises C-rich stars with [Fe/H] < -4.5 and [C/Fe] $\geq +0.7$; Pop IIb contains C-normal stars with [Fe/H] > -4.2 and [C/Fe] $< +0.7$;[18] and in Section 5.5, we shall introduce a toy model that postulates the formation of Pop IIab stars as the result of the coalescence of material from Pop IIa with that of Pop IIb.

5.3 [Fe/H] < −4.5 and [C/Fe] > + 0.7 (Pop IIa)

Only 15 stars are currently known that have [Fe/H] < -4.5. We refer the reader to Frebel & Norris (2015) and references therein for

[17] An estimate of the relative frequency of this type of star is afforded by the work of Thorburn (1994), who reported three of them in a sample of some 80 near-main-sequence stars having $-3.0 <$ [Fe/H] < -1.5 and $T_{\rm eff} > 5500$ K.

[18] We realize that some stars will be excluded by these definitions. Fine tuning will be required as more/better data become available.

Downloaded from https://academic.oup.com/mnras/article/522/1/1358/7095871 by guest on 27 April 2025

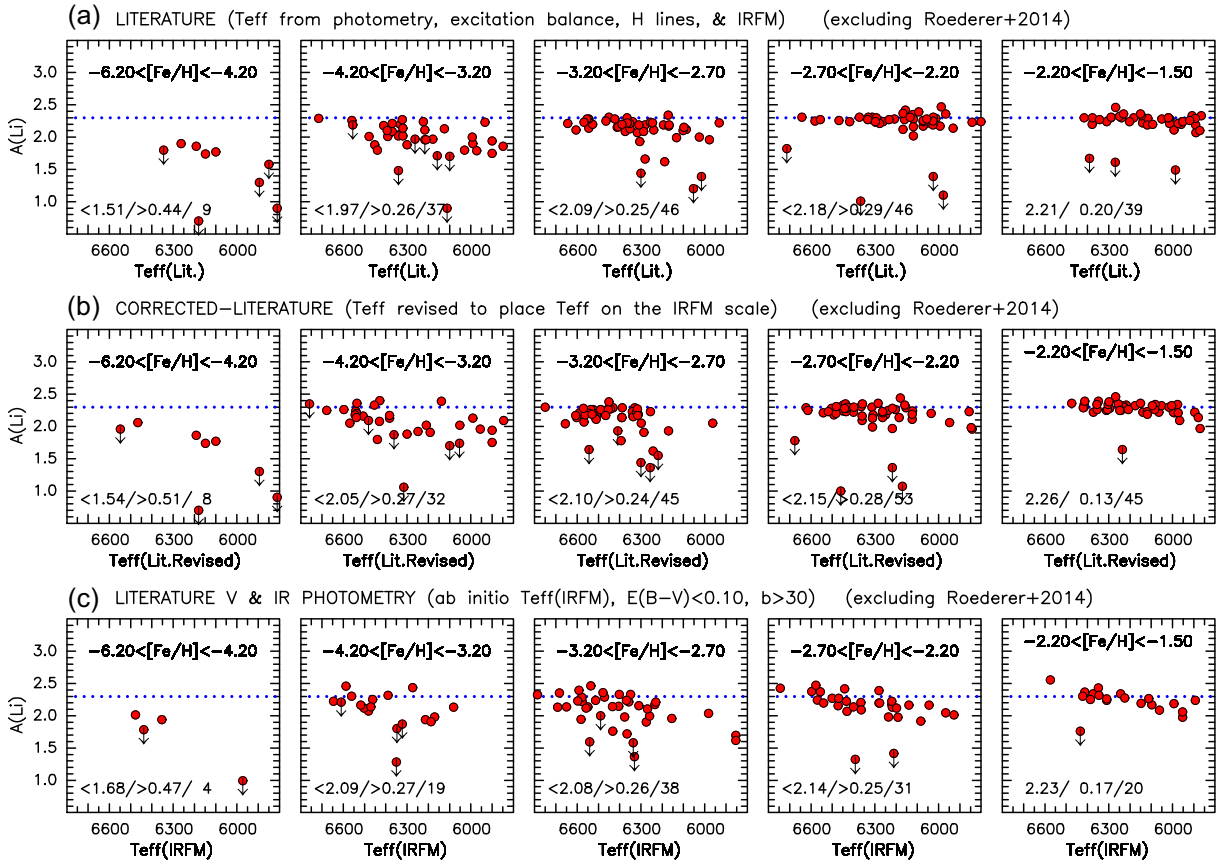

Figure 6. A(Li) versus $T_{\rm eff}$ for (a) the 'Literature', (b) 'Corrected-Literature', and (c) '*ab initio* $T_{\rm IRFM}$' data sets (excluding the Roederer et al. 2014 sample). In the five panels of each row, the range of [Fe/H] is presented towards the top, with [Fe/H] increasing from left to right. At the bottom left of each panel, the three numbers represent the mean A(Li), its dispersion σ, and number of stars.

an extensive literature concerning the chemical enrichment of the metal-free material that emerged following the Big Bang. A short list of topics include minihalos, supermassive rapidly rotating stars, mixing-and-fallback Type II supernovae, Type II supernovae with relativistic jets, and zero-metallicity, rotating, massive intermediate-mass stars. For the present study, we focus on the 8 of those 15 stars with [Fe/H] < -4.5 that lie near the main sequence. Six of them are characterized by large C abundances, with [C/Fe] $\gtrsim$3.5. Their lithium abundances are in the range of $<0.7 <$ A(Li) < 2.1. Depending on their C abundances, low-metallicity stars have been grouped into the 'C-rich' and 'C-normal' objects. Regarding potential formation scenarios of these stars, Chiaki et al. (2017), and others beforehand, e.g. (Frebel et al. 2007), discuss the role of carbon and its critical abundance of $[{\rm C/Fe}]_{\rm b} = 2.30$ that a gas needs to reach in order to cool enough through fine structure lines to lead to low-mass star formation. Below such a critical value, silicate grains would be the dominant coolant instead (Ji, Frebel & Bromm 2014; Chiaki et al. 2017).

The large lithium spread of $<0.7 <$ A(Li) < 2.1, seen in panel (a) of Fig. 10 is at first sight a little surprising. Why is it so large? What is its significance? Meynet et al. (2010) put it very succinctly in their study of CEMP stars: '(Lithium) is completely destroyed in massive stars and also in AGB stars. Thus any mixing of such stellar ejecta with pristine interstellar material will increase the abundance of Li with respect to the abundance in the source material'.

5.3.1 J0023 + 0307 and the Aguado et al. suggestion

Frebel et al. (2019) and Aguado et al. (2019), in their studies of J0023 + 0307[19] ([Fe/H] < -5.8, A(Li) = 1.9, and [C/Fe] > 3.8), discuss different sources of the 'pristine interstellar material'. Frebel et al. (2019) conclude 'the dilution masses inferred here strongly suggest that J0023 + 0307 is a second-generation star formed by recollapse in a Population III minihalo'. Aguado et al. (2019) reach the conclusion that J0023 + 0307 and other stars in the range $-6.0 <$ [Fe/H] < -2.5 provide an upper A(Li) envelope having 'a nearly constant value' and that 'it is unlikely that such uniformity is the result of depletion processes in stars from a significantly higher initial Li abundance but suggests instead a lower primordial production'.

The Aguado et al. (2019) suggestion brings to mind a potentially similar puzzle involving the red giant SM 0313–6708 – the most [Fe/H]-poor star currently known [$T_{\rm eff} = 5125$ K, log $g = 2.3$, [Fe/H] < -7.3, [C/Fe] > 4.9, and A(Li) = 0.7 (Keller et al. 2014)]. Frebel & Norris (2015, see their section 3.6 and fig. 6) project the observed A(Li) backwards in time from the red giant branch to the value the star would have had on the main sequence, and report $A(Li)_{\rm MS} \sim 2.0$. This is not unlike the A(Li) value of the upper Li envelope highlighted by Aguado et al. (2019) of A(Li) $\sim$ 2.0 [and 1.9 (Aguado et al. 2019) and 1.7 (Frebel et al. 2019) for J0023 + 0307 specifically]. Clearly, more accurate observational data on the upper

[19]J0023+0307 = SDSS J002314.00 + 030758.0

Downloaded from https://academic.oup.com/mnras/article/522/1/1358/7095871 by guest on 27 April 2025

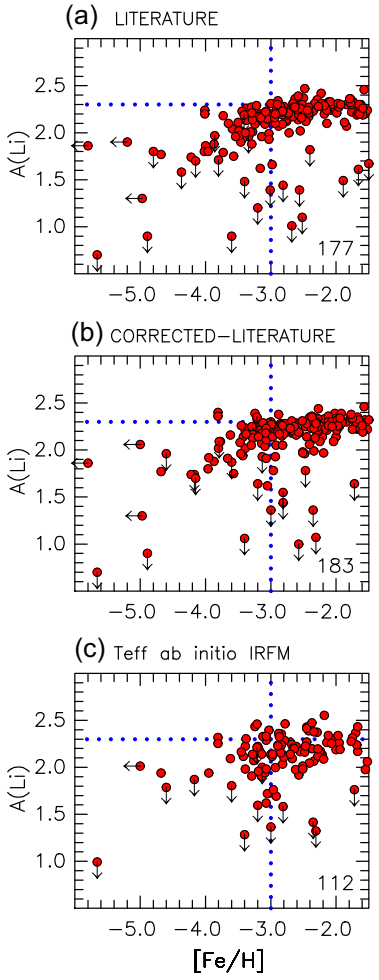

Figure 7. A(Li) versus [Fe/H] for the (a) 'Literature', (b) 'Corrected-Literature', and (c) '*ab initio* $T_{\rm IRFM}$' data sets (excluding the Roederer et al. 2014 sample). The number of stars is given at the bottom right of each panel.

Table 5. Average 'Corrected-Literature' A(Li) and [Fe/H] data from Fig. 6.

⟨A(Li)⟩ (1)	σ(A(Li)) (2)	⟨[Fe/H]⟩ (3)	N[1] (4)
1.536	0.509	−4.977	8
2.049	0.265	−3.556	32
2.097	0.239	−2.977	45
2.155	0.279	−2.448	53
2.264	0.127	−1.864	45

Note. [1]Number of stars

envelope of the lithium distribution, in the range of [Fe/H] < -2.5, are needed to further investigate this important matter and to possibly settle the discussion of whether the primordial lithium abundance is perhaps environment dependent.

5.4 Fu et al. (2015) 'from pre-main sequence to the Spite Plateau' (–4.2 < [Fe/H] < −1.5, Pop IIb)

A basic feature of Population II is the Metallicity Distribution Function (MDF), which, according to Da Costa et al. (2019, see also references therein), 'has a power-law slope of Δ(Log N)/Δ([Fe/H]) $= 1.5 \pm 0.1$ dex per dex for $-4.0 \leq$ [Fe/H] ≤ -2.75 but appears

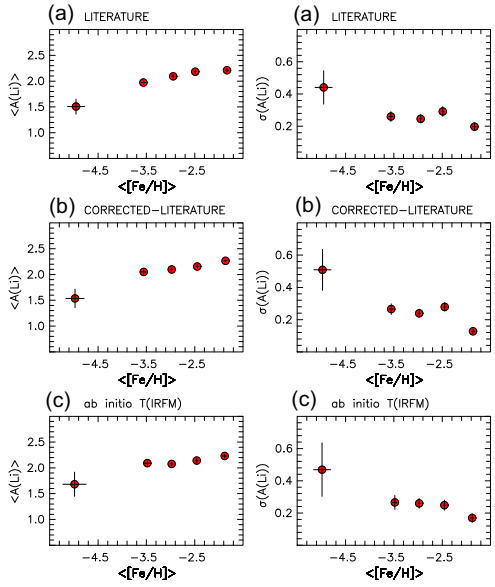

Figure 8. Averages ⟨A(Li)⟩ (Left) and dispersions, σ(A(Li)) (Right) versus ⟨[Fe/H]⟩ for stars in the five horizontal 'Corrected-Literature' panels of Fig. 6.

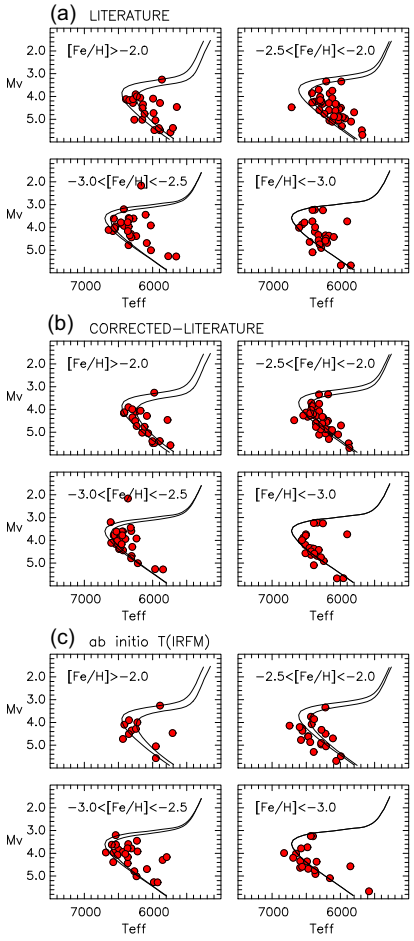

Figure 9. (M_V, $T_{\rm eff}$) – CMDs for (a) the 'Literature', (b) 'Corrected-Literature', and (c) '*ab initio* $T_{\rm IRFM}$' data sets. In each set the four subpanels pertain to stars within the indicated [Fe/H] limits. Also presented are Yale-Yonsei Isochrones for these [Fe/H] values, helium abundance Y = 0.23, [α/Fe] = 0.3, and Age = 12 Gyr.

Downloaded from https://academic.oup.com/mnras/article/522/1/1358/7095871 by guest on 27 April 2025

Table 6. Five CEMP-no stars near [Fe/H] ∼ −3.0.

Star name (1)	[Fe/H] (2)	[C/Fe] (3)	[Ba/Fe] (4)	A(Li) (5)	Author[1] (6)
CD −24 17504	−3.41	1.10	<−1.05	1.99	1
G 64-12	−3.29	1.07	− 0.07	2.36	2
G 64-37	−3.11	1.12	− 0.36	2.25	2
LA 1410–0555[2]	−3.19	1.53	− 0.33	2.17	3
SD 1424 + 5615[2]	−3.01	1.49	<−0.69	2.14	3

Notes. [1]1 = Jacobson & Frebel (2015), 2 = Placco et al. (2016), 3 = Matsuno et al. (2017b); [2]LA 1410–0555 = LAMOST J1410–0555, SD 1424+5615 = SDSS J1424 + 5615.

Table 7. [C/Fe] for 78 near-main-sequence stars over three abundance ranges.

Star name (1)	$T_{\rm eff}$ (2)	[Fe/H] (3)	A(Li) (4)	[C/Fe] (5)	Author[1] (6)
		[Fe/H] < −4.5			
SD 0023 + 0307	6192	<−5.80	1.86	>3.77	AGFR
HE 0233–0343	6100	− 4.68	1.77	3.48	HA15
SD 0929 + 0238	5894	<−4.97	<1.30	>4.24	CA16
SD 1029 + 1729	5811	− 4.89	<0.90	<1.00	CA12
SD 1035 + 0641	6466	<−5.00	2.06	>3.73	BO18
HE 1327–2326	6180	− 5.66	<0.70	4.13	FR08
Pr 221.8 + 09.7	5792	− 4.66	1.70	<1.83	ST18
SD 1742 + 2531	6549	− 4.60	<1.96	3.43	BO15
		−4.2 < [Fe/H] ≤ −3.0			
CS 29527-015	6541	− 3.41	2.24	1.13	BO09
CS 30339-069	6337	− 3.05	2.16	0.62	BO09
CS 22188-033	6243	− 3.05	1.62	<0.84	MP21
SD 0120–1001	5846	− 3.77	2.09	<1.81	MA17
SD 0140 + 2344	6052	− 3.80	2.02	2.00	BO18
HE 0148–2611	6568	− 3.14	2.07	<1.16	MP21
CS 22958-042	6409	− 3.13	<1.93	3.15	SI06
SD 0212 + 0137	6537	− 3.39	2.20	2.08	BO15
		−3.0 < [Fe/H] ≤ −2.0			
BS 17570-063	6298	− 2.92	2.05	0.49	BO09
CS 22882-027	6676	− 2.47	<1.78	<0.24	MP21
CS 29514-007	6313	− 2.86	2.19	<0.76	MP21
CS 22953-037	6526	− 2.84	2.26	0.41	BO09
CS 31061-032	6400	− 2.61	2.22	0.68	BO09
LP 651-4	6489	− 2.79	2.26	0.57	NO19
G 4-37	6308	− 2.57	2.18	0.60	NO19
HD 19445	6087	− 2.01	2.27	0.45	TO92

Notes. [1]AGFR = Aguado et al. (2019), Frebel et al. (2019), AL15 = Alexeeva & Mashonkina (2015), BA05 = Barklem et al. (2005), BO09 = Bonifacio et al. (2009), BO15 = Bonifacio et al. (2015), BO18 = Bonifacio et al. (2018), CA11 = Caffau et al. (2011), CA16 = Caffau et al. (2016), FR08 = Frebel et al. (2008), HA15 = Hansen et al. (2015), JA15 = Jacobson & Frebel (2015), LA08 = Lai et al. (2008), LI15 = Li et al. (2015), MA17 = Matsuno et al. (2017a, b), NO19 = Norris & Yong (2019), PL16 = Placco et al. (2016), ST18 = Starkenburg et al. (2018), SI06 = Sivarani et al. (2006), TO92 = Tomkin et al. (1992)
This table is published in its entirety in the electronic edition of the paper. A portion is shown here for guidance regarding its form and content.

to drop abruptly at [Fe/H] ∼ −4.2, in line with previous studies'. The number of C-rich stars with [Fe/H] < −4.5 falls well above the extrapolation of this MDF.

The majority of Population II is C-normal, with [C/Fe] < 0.7. For stars with [Fe/H] < −1.0, however, C-rich objects ([C/Fe] > 0.7) embrace the CEMP classification of Beers & Christlieb (2005) and Aoki et al. (2007), and the fraction of these stars increases as [Fe/H] decreases. Below [Fe/H] = −3.0, C-rich stars comprise some 20–40 per cent of Population II material (Yong et al. 2013b; Placco et al. 2014).

Fu et al. (2015) propose that the evolution of pre-main-sequence stars provides the site of the astration of primordial lithium. They adopt modifications to standard theory that involve variations in the effects of envelope overshooting, residual mass accretion, EUV-photoevaporation, and main sequence diffusion and Li burning. Adopting conventional nuclear burning and microscopic diffusion along the main sequence, and beginning with the primordial lithium abundance, $A(Li)_P = 2.72$, they reproduce the Spite Plateau for stars in the metallicity range [M/H] = −3.2 to −1.5. Fu et al. (2015) state, 'For our standard choice of parameters, stars with initial mass from m_0 = 0.62 to 0.80 $M/M_\odot$, nicely populate the Spite plateau (A(Li) ∼ 2.26)'. They also foreshadow 'the possibility to interpret the decrease of Li abundance in EMP stars'. We shall assume that the Fu et al. (2015) hypothesis is the most likely stellar-evolutionary explanation of the Spite Plateau in this [Fe/H] abundance range, and for what follows remind the reader that we refer to C-normal stars with [Fe/H] > −4.2 and [C/Fe] < 0.7 as Pop IIb.

One will also see the potential overabundance of riches within the current and previous subsections, given the conflict between the suggestions of Fu et al. (2015), on the one hand, and Aguado et al. (2019), on the other. Said differently, there appears to be potential tension between stellar physics, on the one hand, and cosmological physics, on the other. We shall return to this possibility in Section 6.

5.5 A toy model to explain CEMP-no stars and the Li 'Meltdown' in the range −4.2 < [Fe/H] < −3.0 (Pop IIab)

In Norris & Yong (2019), we presented a toy model that sought to describe the formation of CEMP-no stars in the abundance range $-4.0 \lesssim$ [Fe/H] $\lesssim -2.0$ as the result of the coalescence of gas clouds from the two populations that followed the chemical enrichment by the first zero-heavy-element stars, namely the C-rich, ultra- and hyper-metal-poor (UMP and HMP) population with [Fe/H] < –4.5, on the one hand, and the C-normal, EMP halo stars having [Fe/H] $\gtrsim$ −4.0, on the other.

We refer the reader to Norris & Yong (2019, section 8) and references therein for more details. Suffice it here to repeat the basic premise: 'The first generation of stars produced an initially carbon-rich environment in which further star formation proceeded along two principal pathways, one forming extremely carbon-rich objects (seen today as the C-rich stars with [Fe/H] $\lesssim$ −4.5; the minority population), the other (later) one comprising C-normal stars (seen today as the bulk of stars with [Fe/H] $\gtrsim$ −4.0 – the majority population)'. The simplicity of the model, and the uncertainty of the Fe and C abundance distributions and mass function of the HMP population notwithstanding, the model produced behaviour in the A(C) and [C/Fe] versus [Fe/H] planes not unlike that seen in the Yoon et al. (2016) CEMP Groups I, II, and III. In the present toy-model context, the C-rich, [Fe/H] < −4.5 clouds are responsible for producing Pop IIa, while the C-normal, [Fe/H] $\gtrsim$ −4.0 clouds lead to the formation of Pop IIb. We now investigate to what extent this simple model might explain the apparent sub-Spite Plateau Li abundances of stars with [Fe/H] $\gtrsim$ −4.2 seen in our Figs 2, 4, and 7.

The basic assumption of our toy model model is that the final mass of a putative composite star will be the sum of mass contributions arising from two independent star forming gas clouds. One cloud would have a C-normal chemical environment, the other would be

Downloaded from https://academic.oup.com/mnras/article/522/1/1358/7095871 by guest on 27 April 2025

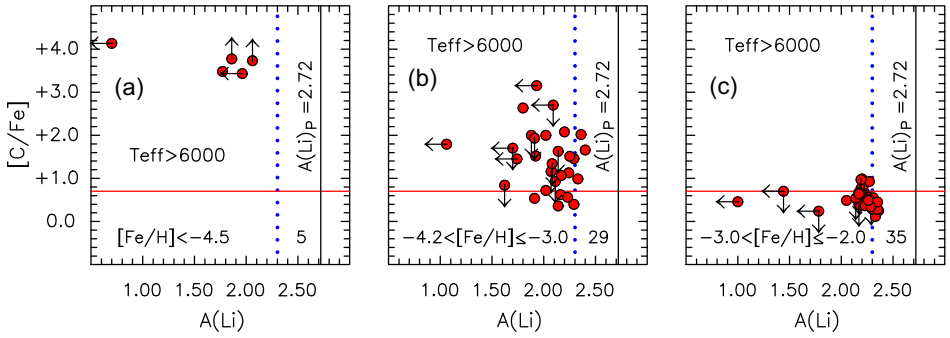

Figure 10. [C/Fe] versus A(Li) for stars with (a) [Fe/H] <-4.5, (b) $-4.2 <$ [Fe/H] ≤ -3.0, and (c) $-3.0 <$ [Fe/H] ≤ -2.0, for stars with $T_{\rm eff} > 6000$ K. The number of stars is presented at the bottom right. Black vertical lines represent Primordial Lithium ($A(Li)_P = 2.72$), the red line at A(Li) = 0.7 separates C-weak and C-strong stars, and the blue dotted lines are for reference purposes.

a C-rich environment. To construct such a star, we then require gas mass contributions from each cloud with their respective chemical compositions. We draw each of said gas mass contributions at random from the Salpeter mass function but restricted to the range of $0.10 \leq M/M_{\odot} \leq 0.75$. To approximate the existence of 12-13 Gyr metal-poor stars with [Fe/H] < -2.0 now lying near the main-sequence turnoff, we then require that the composite star have a final mass in the range of $0.65 \leq M/M_{\odot} \leq 0.75$.

Having fixed the abundances of each of the randomly chosen contributing masses, we then determine the chemical abundances of Fe, C, and Li of the composite star. Details are further discussed below.

We note that a basic shortcoming of our toy model pertains to the lower limit on the lesser of the two gas mass contributions to a composite star. This 0.1 $M_{\odot}$ limit is not well constrained, and smaller contributions may occur in reality. The distribution of relative contributions is also unknown. Consequently, computational conveniences – the 0.1 $M_{\odot}$ lower limit and the Salpeter IMF – have been adopted. Within these caveats some insights may still be gained and some progress may be possible.

In addition, the model is agnostic to the details concerning the formation process and location of the putative composite star. However, the idea that two gas mass reservoirs contribute to the making of a star is not new. Recently, a version of it was explored by Smith et al. (2015) who modelled external enrichment by a neighbouring minihalo. The basic scenario follows a minihalo in the early Universe that becomes chemically enriched by a neighbouring minihalo whose massive supernova injects metals at high speed into it. Such a scenario has also been suggested to explain the different populations of C-rich and C-normal stars (Ezzeddine et al. 2019), assuming that significant amounts of carbon produced by a hypernova were acquired by an Fe-poor minihalo. In these cases the external enrichment scenario is naturally limited to very early, low-metallicity environments, consistent with the approach adopted in the present study.

5.5.1 The composite Pop IIab

In Section 5.2, we defined three Population II subpopulations: (1) Pop IIa (the C-rich stars with [Fe/H] < -4.5), (2) Pop IIb (the C-normal stars with [Fe/H] > -4.2), and (3) Pop IIab (composites of material of these two subpopulations).

Assuming that the toy-model predictions would best represent 3D,NLTE observational values, rather than 1D,LTE, we re-define our model parameters accordingly. Given the small number of observed stars with [Fe/H < -4.5, we have adopted representative population parameters of $[Fe/H]_{3D,\,NLTE} = -5.00$, $A(Li)_{3D,\,NLTE} = 0.00$, and $[C/Fe]_{3D,\,NLTE} = 3.50$; and for the C-normal Pop IIb we adopt a modified Yong et al. (2013b) MDF over the range $-4.0 < [Fe/H]_{3D,\,NLTE} < -2.0$, together with $A(Li)_{3D,\,NLTE} = 2.30$, and $[C/Fe]_{3D,\,NLTE} = 0.30$. For each $M_{C\text{-rich}}$, $M_{C\text{-normal}}$ combination of the composite star, the Pop IIab $[Fe/H]_{3D,\,NLTE}$ and $[C/Fe]_{3D,\,NLTE}$ values then follow. We use transformations based on Norris & Yong (2019) to obtain 1D,LTE predictions[20] for comparison with the observational results in Fig. 10.

It is these composite stars that we refer to above as Pop IIab. By definition, Pop IIab has two components: in one, which we shall call Pop IIaba, the larger fraction of each star comprises (C-rich) Pop IIa material; and in the second, Pop IIabb, the larger fraction consists of (C-normal) Pop IIb material. The significance of the subdivision is that Pop IIaba will on average have higher [C/Fe] and lower A(Li) values than those of Pop IIabb, and vice-versa. This difference drives the two subpopulations apart in the A(Li) and [C/Fe] versus [Fe/H] planes.

Fig. 11 presents this example of the behaviour of the three subpopulations Pop IIb, Pop IIaba, and Pop IIabb in the $A(Li)_{1D,\,LTE}$ and $[C/Fe]_{1D,\,LTE}$ versus $[Fe/H]_{1D,\,LTE}$ planes, and that of $[C/Fe]_{1D,\,LTE}$ versus $A(Li)_{1D,\,LTE}$. (We have added Gaussian errors of 0.05, 0.10, and 0.15 dex to the model A(Li), [Fe/H], and [C/Fe] values, respectively). While we have no means of determining the relative numbers of the three subpopulations, by way of example, we have plotted the positions of 20 toy-model stars in each of the upper three rows of the figure, together with their co-addition in the bottom row. In the figure, the left column contains $A(Li)_{1D,\,LTE}$ versus $[Fe/H]_{1D,\,LTE}$, the middle column presents $[C/Fe]_{1D,\,LTE}$ versus $[Fe/H]_{1D,\,LTE}$, and on the right we plot $[C/Fe]_{1D,\,LTE}$ versus $A(Li)_{1D,\,LTE}$. From top to bottom, each column contains Pop IIb (C-normal), Pop IIabb (composite stars dominated by (C-normal) Pop IIb), Pop IIaba (composites dominated by (C-rich) Pop IIa), and Pop IIb + Pop IIabb + Pop IIaba (their co-addition), respectively.

We are encouraged to suggest that there is a significant similarity between the $A(Li)_{1D,\,LTE}$ versus $[Fe/H]_{1D,\,LTE}$ co-added panel (d) in Fig. 11 and the observed abundance distributions in Fig. 7. It

[20] $[Fe/H]_{1D,\,LTE} = [Fe/H]_{3D,\,NLTE} - 0.35$ and $[C/H]_{1D,\,LTE} = [C/H]_{3D,\,NLTE} - 0.17[Fe/H]_{3D,\,NLTE} - 0.09$.

Downloaded from https://academic.oup.com/mnras/article/522/1/1358/7095871 by guest on 27 April 2025

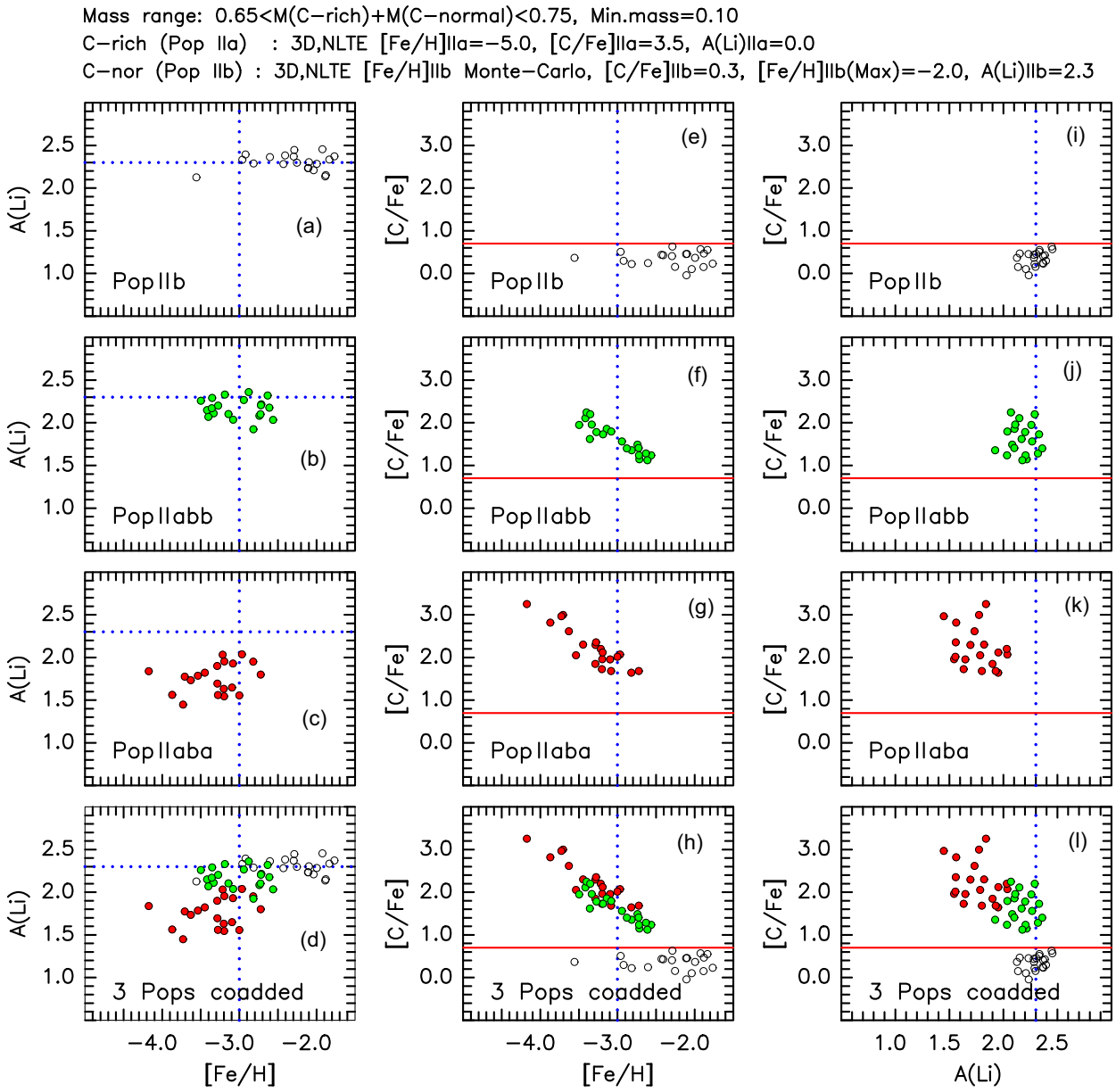

Figure 11. (Left) $A(Li)_{1D,\,LTE}$ versus $[Fe/H]_{1D,\,LTE}$, (Middle) $[C/Fe]_{1D,\,LTE}$ versus $[Fe/H]_{1D,\,LTE}$, and (Right) $[C/Fe]_{1D,\,LTE}$ versus $A(Li)_{1D,\,LTE}$ for the toy-model three Population II subpopulations. From top to bottom, the panels present Pop IIb = C-normal halo, Pop IIabb = C-normal dominated component, Pop IIaba = C-rich dominated component, and the co-addition of Pop IIb, Pop IIabb, and Pop IIaba. See text for discussion.

is perhaps all that one might hope for, insofar as the observed sample is also very statistically incomplete, as the result of selection effects. Perhaps the most interesting aspect of the toy model, however, is the prediction that Pop IIaba and Pop IIabb will occupy somewhat different regions of the diagram in the vicinity of [Fe/H] = −3.0. In particular, concerning the report by Matsuno et al. (2017b) that there are CEMP-no stars with A(Li) = 2.1–2.2 (see our Table 6), perhaps these stars belong to the toy-model composite Pop IIabb, in which there is a dominance of Pop IIb material.

There also appears to be a significant similarity between the $[C/Fe]_{1D,\,LTE}$ versus $A(Li)_{1D,\,LTE}$ panels (i)–(l) in Fig. 11 on the one hand, and the observed abundance distributions in Fig. 10 on the other.

5.5.2 *Caveat emptor*

These selected favourable comparisons notwithstanding, we hasten to acknowledge that the toy model is at best only suggestive. There are many free parameters in our presentation – for example, the single C-rich Pop IIa component represented by only one set of parameters,[21] the mass ranges of the two clouds that coalesce (also the assumption that there is no mass loss when they combine), and the [Fe/H] range of the Pop IIb clouds. Our aim here is to show that one can find a set of parameters that appears to reproduce the observational data. We hope that other authors, theoretically inclined,

[21] See Norris & Yong (2019, figs 9–11) for changes that occur when different Pop IIa parameters are adopted.

Downloaded from https://academic.oup.com/mnras/article/522/1/1358/7095871 by guest on 27 April 2025

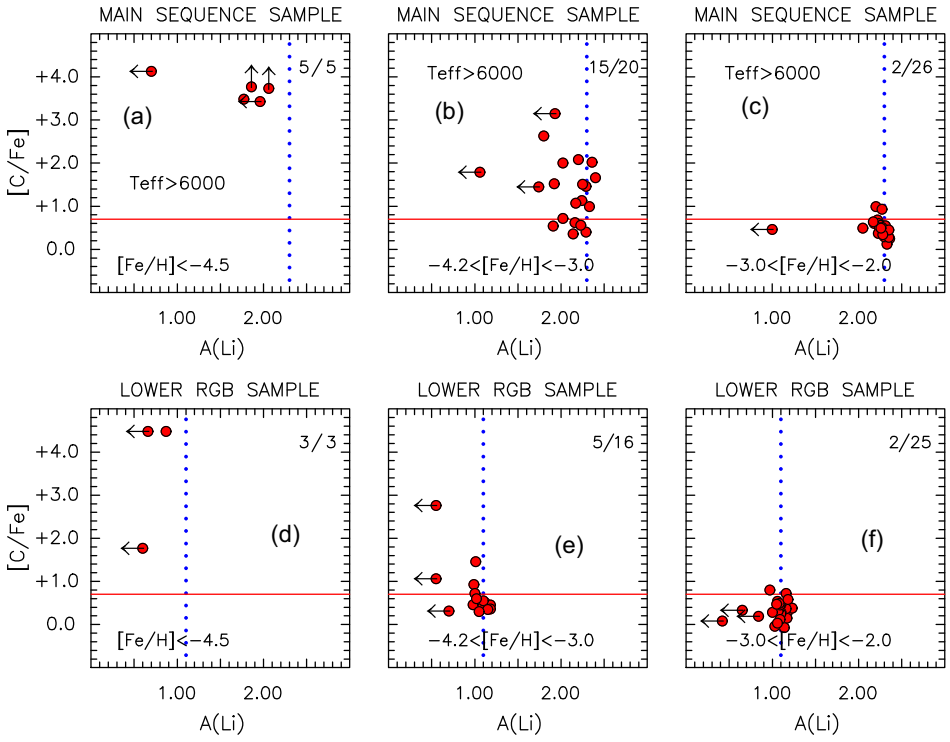

Figure 12. [C/Fe] versus A(Li) for stars with (Left) [Fe/H] < -4.5, (Middle) $-4.2 <$ [Fe/H] ≤ -3.0, and (Right) $-3.0 <$ [Fe/H] ≤ -2.0. The upper and lower panels present data for main sequence ($T_{\rm eff} > 6000$ K) and LRGB stars, respectively. At top right of each panel the two numbers form the ratio of the number of C-rich stars to the total number of stars (excluding the stars with upper limits). The black vertical lines represent Primordial Lithium ($A(Li)_P = 2.72$), the red line at A(Li) = 0.7 separates C-weak and C-strong stars, and the blue dotted lines are for reference purposes. See text for details.

will accept the challenge to investigate in more detail the concept we have proposed.

5.6 The sloping of the Spite Plateau

We conclude our discussion by recalling that while in Section 1 we suggested there are five lithium problems, we have so far not discussed one of them – the slope of the Li plateau in the (A(Li), [Fe/H]) – plane in the range $-3.5 \lesssim$ [Fe/H] $\lesssim -1.5$ (other than to quantify its value in Figs 2 and 4). Examination of panels (a)–(d) of Fig. 11 suggests that a thin and horizontal plateau of Pop IIb stars merging with Pop IIab stars, at [Fe/H] $\sim -3.0 - -2.5$, could provide a simple explanation.

In Section 3.4, we presented the average values and dispersions of A(Li) for stars with $T_{\rm eff} > 6000$ K and noted that for those in the range $-2.2 <$ [Fe/H] < -1.7 (within the Spite & Spite (1982) discovery range), the plateau appears horizonal in the A(Li) versus $T_{\rm eff}$ regime of the 'Literature' and 'Corrected-Literature' panels. To investigate this suggestion further, we considered the lithium parameters of the Spite Plateau in the range $-2.0 <$ [Fe/H] < -1.0, using the data for the 36 stars in the intersection of the Asplund et al. (2006) and Meléndez et al. (2010) samples, which we regard to be of the highest quality within this abundance range. We find $\langle A(Li)\rangle = 2.322 \pm 0.013$, with $\sigma(A(Li)) = 0.078$, resulting from 35 stars (one 3σ outlier having been omitted). We would also draw the reader's attention to the fact that CEMP-no stars are found only below [Fe/H] $= -2.0$ (Aoki 2010; Norris et al. 2013), supporting the above suggestion of the merger of two subpopulations.

6 SUMMARY

We have collated and discussed literature lithium abundances of some 200 near-main-sequence stars with $T_{\rm eff} > 5800$ K and [Fe/H] < -1.5. Three different approaches to the data were explored: (1) adopt 'Literature' values – the data remain unchanged; (2) homogenize the data to obtain 'Corrected-Literature' values – moving the data onto a single stellar temperature (IRFM) scale, and (3) determine '*ab initio* IRFM $T_{\rm IRFM}$' values – IRFM temperatures from literature infrared colours.

We then examined A(Li) as a function of $T_{\rm eff}$, [Fe/H], and [C/Fe]. In Section 1, five aspects of the complicated distribution of stars in the (A(Li), [Fe/H]) plane were identified, which challenge insight into the status of lithium abundances at the earliest times. We conclude here with a summary of the potential implications of these five problems.

(i) Very low A(Li) values in the group of stars related to 'blue stragglers'

This is a minority ∼5 per cent population, noted by Bonifacio et al. (2012) to be restricted to relatively high [Fe/H] values, suggesting these stars are not relevant to lithium abundance patterns at the earliest times.

(ii) Lithium in the most iron-poor stars ([Fe/H] < -4.5)

These are the first stars following Population III and the oldest Population II objects (which we designate Pop IIa) – lithium-poor ($<0.5 <$ A(Li) < 2.1) and extremely carbon-rich (most having [C/Fe] $\gtrsim$3.5). They formed earliest at the epoch when carbon grains were the dominant gas coolant. Aguado et al. (2019) suggest there are stars in the range $-6.0 <$ [Fe/H] < -2.5 that provide an upper A(Li)

Downloaded from https://academic.oup.com/mnras/article/522/1/1358/7095871 by guest on 27 April 2025

envelope 'at a nearly constant value' of A(Li) $\sim$ 2.0. They argue this value is the Primordial Lithium Abundance.

(iii) Lithium 'Meltdown' in stars in the range $-4.2 <$ [Fe/H] < -3.0

The second and later pathway of star formation, in which silicate grains are the dominant gas coolants, leads to C-normal population stars, seen today as the bulk of stars with [Fe/H] $\gtrsim -4.2$ (which we call Pop IIb). We presented a toy model in which gas from Pop IIa and Pop IIb combine to form Population II stars that we call Pop IIab, which form a large part of the 'meltdown', and in which there is an anticorrelation between lithium and carbon. That is, the lithium 'meltdown' is accompanied by carbon enrichment, with [C/Fe] values as large as [C/Fe] = +2.0 to +3.0.

(iv) The slope of the Spite Plateau in the A(Li) versus [Fe/H] plane

Over the range $-3.5 <$ [Fe/H] < -1.5, the sloping of the Spite Plateau appears to be caused by the merging of two subpopulations. The first constitutes a plateau of C-normal Pop IIb stars that have $\langle$A(Li)$\rangle = 2.322 \pm 0.013$ over the range $-2.0 <$ [Fe/H] < -1.0. The second is the subpopulation of C-rich Pop IIab stars. The latter resulted from the combination of C-rich and strongly Li-depleted (Pop IIa) and C-normal (Pop IIb) material.

(v) The primordial lithium problem

Fu et al. (2015) propose pre-main-sequence evolution as the site of the astration of primordial lithium. Their model explains the Spite Plateau in the metallicity range [M/H] = -3.2 to -1.5, and for their 'standard choice of parameters, stars with initial mass from m_0 = 0.62 to 0.80 $M/M_\odot$, nicely populate the Spite Plateau (A(Li) $\sim$ 2.26)'.

According to Cyburt et al. (2008), the primordial lithium abundance is $A(Li)_P = 2.72 \pm 0.06$, compared with an observed value A(Li) $= 2.09 \pm 0.03$. Our updated $\langle$A(Li)$\rangle$ value is 2.322 ± 0.013. [Note that the more recent Planck Collaboration VI (2020) CMB results 'do not discuss other light elements, such as... lithium... and do not shed any further light on earlier CMB experiments.']

In Section 5, we cited (1) the suggestion of Aguado et al. (2019) that stars in the range $-6.0 <$ [Fe/H] < -2.5 provide an upper lithium abundance envelope at nearly constant value A(Li) $\sim$ 2.0, 'suggesting a lower primordial production' than the currently accepted value; and (2) the most [Fe/H]-poor star currently known – the red giant SM 0313–6708, with [Fe/H] < -7.3, log $g = 2.3$, [C/Fe] > 4.9, and A(Li) = 0.7 (Keller et al. 2014) – is suggested by Frebel & Norris (2015) to have had A(Li) $\sim$ 2.0 when on the main sequence.

Given this tension between lithium abundances based on stellar and cosmological endeavours, it is then of considerable interest that Riess et al. (2019) report conflicting Hubble Constants (H_0) of 74.03 ± 1.42 km s^{-1} Mpc^{-1} (from local observations) compared with 67.4 ± 0.5 km s^{-1} Mpc^{-1} (inferred from Planck CMB (Planck Collaboration VI 2020) plus Big Bang ΛCDM) – a difference of 6.6 ± 1.5 km s^{-1} Mpc^{-1}. A similar, independent, conclusion has also been reached by Freedman et al. (2019). That is, there are tensions between stellar- and cosmological-based estimates of both the primordial lithium abundance and the Hubble Constant.

With this in mind, we noted in Section 5 that more observational data on the upper envelope of the lithium distribution in the abundance range $-6.0 <$ [Fe/H] < -2.5 are needed to address the lithium aspect of these issues.

ACKNOWLEDGEMENTS

J.E.N. acknowledges Constantine Deliyannis for his insistence in the late 1990s that 'there are cases of well-observed stars, which cannot have the same Li abundance' (see Ryan et al. 1996), as proved to be the case. We thank Piercarlo Bonificacio for his comments on the manuscript, in particular for alerting us to the work of, and his comments on, Mucciarelli et al. (2022). Parts of this research were supported by the Australian Research Council Centre of Excellence for All Sky Astrophysics in 3 Dimensions (ASTRO 3D), through project number CE170100013. A.F. acknowledges support from NSF grant AST-1716251. This work has made use of data from the European Space Agency (ESA) mission *Gaia* (https://www.cosmos.esa.int/gaia), processed by the *Gaia* Data Processing and Analysis Consortium (DPAC, https://www.cosmos.esa.int/web/gaia/dpac/consortium). Funding for the DPAC has been provided by national institutions, in particular the institutions participating in the *Gaia* Multilateral Agreement.

DATA AVAILABILITY

The data underlying this article will be shared on reasonable request to the corresponding author.

REFERENCES

Aguado D. S., González Hernández J. I., Allende Prieto C., Rebolo R., 2019, ApJ, 874, L21
Alexeeva S. A., Mashonkina L. I., 2015, MNRAS, 453, 1619
Aoki W., 2010, in Cunha K., Spite M., Barbuy B., eds, Proceedings IAU, 265, Chemical Abundances in the Universe: Connecting First Stars to Planets. Cambridge Univ. Press, Cambridge, p. 111
Aoki W. et al., 2006, ApJ, 639, 897
Aoki W., Beers T. C., Christlieb N., Norris J. E., Ryan S. G., Tsangarides S., 2007, ApJ, 655, 492
Aoki W., Barklem P. S., Beers T. C., Christlieb N., Inoue S., Garcia Pérez A. P., Norris J. E., Carollo D., 2009, ApJ, 698, 1803
Aoki W., Ito H., Tajitsu A., 2012, ApJ, 751, L6
Asplund M., 2005, ARA&A, 43, 481
Asplund M., Carlsson M., Botnen A. V., 2003, A&A, 399, L31
Asplund M., Lambert D. L., Nissen P. E., Primas F., Smith V. V., 2006, ApJ, 644, 229
Asplund M., Grevesse N., Sauval A. J., Scott P., 2009, ARA&A, 47, 481
Barklem P. S. et al., 2005, A&A, 439, 129
Beers T. C., Christlieb N., 2005, ARA&A, 43, 531
Bonifacio P. et al., 2009, A&A, 501, 519
Bonifacio P., Sbordone L., Caffau E., Ludwig H. G., Spite M., González Hernández J. I., Behara N. T., 2012, A&A, 542, A87
Bonifacio P. et al., 2015, A&A, 579, A28
Bonifacio P. et al., 2018, A&A, 612, A65
Bromm V., Loeb A., 2003, Nature, 425, 812
Caffau E. et al., 2011, Nature, 477, 67
Caffau E. et al., 2012, A&A, 542, A51
Caffau E. et al., 2016, A&A, 595, L6
Casagrande L., Ramírez I., Meléndez J., Bessell M., Asplund M., 2010, A&A, 512, A54
Chiaki G., Tominaga N., Nozawa T., 2017, MNRAS, 472, L115
Cyburt R. H., Fields B. D., Olive K. A., 2008, J. Cosmol. Astropart. Phys., 11, 12
Da Costa G. S. et al., 2019, MNRAS, 489, 5900
Deliyannis C. P., Demarque P., Kawaler S. D., 1990, ApJS, 73, 21
Demarque P., Woo J.-H., Kim Y.-C., Yi S. K., 2004, ApJS, 155, 667
Dunkley J. et al., 2009, ApJS, 180, 306
Ezzeddine R. et al., 2019, ApJ, 876, 97
Fields B. D., 2011, Annu. Rev. Nucl. Par. Sci., 61, 47
Fields B. D., Molaro P., Sarkar S., 2014, preprint (arXiv:1412.1408)
Ford A., Jeffries R. D., Smalley B., Ryan S. G., Aoki W., Kawanomoto S., James D. J., Barnes J. R., 2002, A&A, 393, 617
Frebel A., Norris J. E., 2015, ARA&A, 53, 631
Frebel A. et al., 2005, Nature, 434, 871
Frebel A., Johnson J. L., Bromm V., 2007, MNRAS, 380, L40

Downloaded from https://academic.oup.com/mnras/article/522/1/1358/7095871 by guest on 27 April 2025

Frebel A., Collet R., Eriksson K., Christlieb N., Aoki W., 2008, ApJ, 684, 588
Frebel A., Ji A. P., Ezzeddine R., Hansen T. T., Chiti A., Thompson I. B., Merle T., 2019, ApJ, 871, 146
Freedman W. L. et al., 2019, ApJ, 882, 34
Fu X., Bressan A., Molaro P., Marigo P., 2015, MNRAS, 452, 3256
Fulbright J. P., 2000, AJ, 120, 1841
Gaia Collaboration 2016, A&A, 595, A1
Gaia Collaboration 2021, A&A, 649, A1
González Hernández J. I. et al., 2008, A&A, 480, 233
Goswami P. P., Goswami A., 2022, A&A, 657, A50
Hakkila J., Myers J. M., Stidham B. J., Hartmann D. H., 1997, AJ, 114, 2043
Hansen T. et al., 2015, ApJ, 807, 173
Henden A. A., Templeton M., Terrell D., Smith T. C., Levine S., Welch D., 2016, VizieR Online Data Catalog, II/336
Honda S., Aoki W., Kajino T., Ando H., Beers T. C., Izumiura H., Sadakane K., Takada-Hidai M., 2004, ApJ, 607, 474
Jacobson H. R., Frebel A., 2015, ApJ, 808, 53
Ji A. P., Frebel A., Bromm V., 2014, ApJ, 782, 95
Keller S. C. et al., 2014, Nature, 506, 463
Lai D. K., Bolte M., Johnson J. A., Lucatello S., Heger A., Woosley S. E., 2008, ApJ, 681, 1524
Lardo C. et al., 2021, MNRAS, 508, 3068
Li H., Aoki W., Zhao G., Honda S., Christlieb N., Suda T., 2015, PASJ, 67, 84
Lucatello S., Tsangarides S., Beers T. C., Carretta E., Gratton R. G., Ryan S. G., 2005, ApJ, 625, 825
Masseron T., Johnson J. A., Plez B., van Eck S., Primas F., Goriely S., Jorissen A., 2010, A&A, 509, A93
Matas Pinto A. M. et al., 2021, A&A, 654, A170
Matsuno T., Aoki W., Beers T. C., Lee Y. S., Honda S., 2017a, AJ, 154, 52
Matsuno T., Aoki W., Suda T., Li H., 2017b, PASJ, 69, 24
Meléndez J., Shchukina N. G., Vasiljeva I. E., Ramírez I., 2006, ApJ, 642, 1082
Meléndez J., Casagrande L., Ramírez I., Asplund M., Schuster W. J., 2010, A&A, 515, L3
Meynet G., Hirschi R., Ekstrom S., Maeder A., Georgy C., Eggenberger P., Chiappini C., 2010, A&A, 521, A30
Mucciarelli A., Monaco L., Bonifacio P., Salaris M., Deal M., Spite M., Richard O. A., Lallement R., 2022, A&A, 661, A153
Norris J. E., 2018, in Chiappini C., Minchev I., Starkenburg E., Valentini M.,eds, Proceedings IAU 334, Rediscovering Our Galaxy. Cambridge Univ. Press, Cambridge, p. 3
Norris J. E., Yong D., 2019, ApJ, 879, 37
Norris J. E., Christlieb N., Korn A. J., Eriksson K., Bessell M. S., Beers T. C., Wisotzki L., Reimers D., 2007, ApJ, 670, 774
Norris J. E. et al., 2013, ApJ, 762, 28
Piau L., Beers T. C., Balsara D. S., Sivarani T., Truran J. W., Ferguson J. W., 2006, ApJ, 653, 300
Placco V. M., Frebel A., Beers T. C., Stancliffe R. J., 2014, ApJ, 797, 21
Placco V. M., Beers T. C., Reggiani H., Meléndez J., 2016, ApJ, 829, L24
Planck Collaboration VI 2020, A&A, 641, A6
Reggiani H., Meléndez J., Kobayashi C., Karakas A., Placco V., 2017, A&A, 608, A46
Richard O., Michaud G., Richer J., 2005, ApJ, 619, 538
Riess A. G., Casertano S., Yuan W., Macri L. M., Scolnic D., 2019, ApJ, 876, 85
Roederer I. U., Preston G. W., Thompson I. B., Shectman S. A., Sneden C., Burley G. S., Kelson D. D., 2014, AJ, 147, 136
Ryan S. G., Beers T. C., Deliyannis C. P., Thorburn J. A., 1996, ApJ, 458, 543
Ryan S. G., Norris J. E., Beers T. C., 1999, ApJ, 523, 654
Ryan S. G., Beers T. C., Kajino T., Rosolankova K., 2001a, ApJ, 547, 231
Ryan S. G., Kajino T., Beers T. C., Suzuki T. K., Romano D., Matteucci F., Rosalankova K., 2001b, ApJ, 549, 55
Ryan S. G., Gregory S. G., Kolb U., Beers T. C., Kajino T., 2002, ApJ, 571, 501
Sandage A., 1986, ARA&A, 24, 421
Sbordone L. et al., 2010, A&A, 522, A26
Sivarani T. et al., 2006, A&A, 459, 125
Smith B. D., Wise J. H., O'Shea B. W., Norman M. L., Khochfar S., 2015, MNRAS, 452, 2822
Spite F., Spite M., 1982, A&A, 115, 357
Spite M., Caffau E., Bonifacio P., Spite F., Ludwig H. G., Plez B., Christlieb N., 2013, A&A, 552, A107
Starkenburg E. et al., 2018, MNRAS, 481, 3838
Thorburn J. A., 1994, ApJ, 421, 318
Tomkin J., Lemke M., Lambert D. L., Sneden C., 1992, AJ, 104, 1568
Wagoner R. V., 1973, ApJ, 179, 343
Wagoner R. V., Fowler W. A., Hoyle F., 1967, ApJ, 148, 3
Yong D. et al., 2013a, ApJ, 762, 26
Yong D. et al., 2013b, ApJ, 762, 27
Yoon J. et al., 2016, ApJ, 833, 20
Zacharias N., Finch C. T., Girard T. M., Henden A., Bartlett J. L., Monet D. G., Zacharias M. I., 2013, AJ, 145, 44

SUPPORTING INFORMATION

Supplementary data are available at *MNRAS* online.

Table 3. Multiple Observations of 'Literature' and 'Corrected-Literature' Data.
Table 4. Averaged 'Literature', 'Corrected-Literature', and '*ab initio* IRFM $T_{\rm eff}$' Data.
Table 7. [C/Fe] for 78 Near-Main-Sequence Stars over Three Abundance Ranges.

Please note: Oxford University Press is not responsible for the content or functionality of any supporting materials supplied by the authors. Any queries (other than missing material) should be directed to the corresponding author for the article.

APPENDIX: A COMPARISON BETWEEN MAIN-SEQUENCE AND LOWER RED GIANT BRANCH LITHIUM ABUNDANCE DISTRIBUTIONS

The final entry in our Table 1 (milestones in the study of lithium abundances) is 'Discovery of a thin lithium plateau among metal-poor red giant branch stars' of Mucciarelli et al. (2022). In this work, its authors report, 'The Lower RGB (LRGB) stars display an A(Li) distribution that is clearly different from that of the dwarfs, without signatures of a meltdown and with two distinct components: (a) a thin A(Li) plateau with an average A(Li) $= 1.09 \pm 0.01$ dex ($\sigma = 0.07$ dex) and (b) a small fraction of Li-poor stars with A(Li) lower than ~ 0.7 dex'.

To investigate the apparent inconsistency between the relative simplicity of the LRGB Li distribution compared to the five lithium problems shown schematically in our Fig. 1 we compare the values presented in the Mucciarelli et al. (2022) table 1 and fig. 2 (their A(Li) versus [Fe/H] and $T_{\rm eff}$) with the data in our Table 7 and Fig. 10. A basic difference between the two approaches is that while fig. 2 of Mucciarelli et al. (2022) centres on A(Li) versus [Fe/H], our Fig. 10 examines the inter-relationship between [Fe/H], [C/Fe], and A(Li). Carbon and iron remain essentially unchanged in the evolutionary transition from main sequence to LRGB.[22] We address the possibility that carbon may be relevant for an understanding of the apparent difference between the above two systematizations.

[22]Placco et al. (2014) show that [C/H] corrections are always less than 0.06 dex for RGB stars having log g > 2.0, the lower limit of the Mucciarelli et al. (2022) sample.

Downloaded from https://academic.oup.com/mnras/article/522/1/1358/7095871 by guest on 27 April 2025

Our first step is to seek to minimize the differences in selection effects between the two approaches. In particular, our analysis included only stars with [Fe/H] ≤ -2.0 as the upper limit of our sample in Fig. 10. We therefore adopt that limit here. Then, given that CEMP-s stars were excluded from the main-sequence group (see our Section 2) the three CEMP stars of Mucciarelli et al. (2022), which are also CEMP-s – CS 29495-042, HE 0207–1423, and HE 1005–1439 – (see Masseron et al. 2010; Yong et al. 2013a and Goswami & Goswami 2022, respectively), are excluded from the present comparison. Finally, following Aoki et al. (2007), we define C-rich stars as those having [C/Fe] > 0.7. With the above restrictions, the Mucciarelli et al. (2022) sample size reduces from 58 to 44 stars, while the number of main-sequence stars in our Table 7 that have $T_{\rm eff}$ > 6000 K changes from 78 to 70. A significant difference between the two data sets is that while all stars in the LRGB group have observed [C/Fe] values, this is not the case for the main-sequence stars, for which 25 have only upper limits. Against this background, we shall initially discuss only those stars with $T_{\rm eff} > 6000$ K in which carbon has been detected.

Fig. 12 presents the results for the two data sets, with the main-sequence sample in the upper three panels and the LRGB stars in the lower three. The format is similar to that in our Fig. 10: [C/Fe] versus A(Li) is plotted for three [Fe/H] regimes, increasing from left to right: (left) [Fe/H] < -4.5, (middle) $-4.2 <$ [Fe/H] ≤ -3.0, and (right) $-3.0 <$ [Fe/H] ≤ -2.0 for both data sets.[23] In all panels, the red line represents [C/Fe] $= 0.70$, above which stars are C-rich; in the upper panels, as in Fig. 10 the dotted blue line represents A(Li) $=$ 2.3, while in the three lower panels A(Li) $= 1.09$, adopted following Mucciarelli et al. (2022).

The numbers in the top right of each panel in the figure represent the ratio of the number of C-rich stars to the total number of stars (excluding those with only upper limiting [C/Fe] values). In the left-most panels, all stars are C-rich, while in the right-most panels, the ratios contain mainly C-normal stars with ratios close to 0.08. The two middle panels are more interesting, both exhibiting significantly large spreads in [C/Fe] values. The ratios of C-rich stars to all stars are very different – for the main-sequence stars the ratio is 0.75 while for the LRGB stars it is 0.31 – but these figures disguise very different selection biases dictated by the temperature- and pressure-differences in the carbon detection limits for (warm) main sequence stars and (cooler) LRGB stars. The LRGB ratio of 0.31 for the C-rich fraction is in excellent agreement with the ratios (fractions) of ∼0.2–0.4 for CEMP-no stars in the abundance range $-3.8 <$ [Fe/H] < -3.0 reported by Yong et al. (2013b, their fig. 7; see also Placco et al. 2014 and references therein).

For the main-sequence group, we have excluded a significant number of stars that have only upper limit estimates for [C/Fe]. In our Fig. 10 one sees that the total number of stars in panel (b) ($-4.2 <$ [Fe/H] ≤ -3.0) (including those with only upper [C/Fe] limits) is 29. If one were to assume that those with upper limit are C-normal, the main-sequence ratio would become $15/29 = 0.52$ – not too far from the mark. The likely explanation of the large ratio for the main-sequence sample is that the data selection procedure adopted here is biased towards stars having CEMP-no characteristics and/or large data samples (see for example Barklem et al. (2005), Jacobson & Frebel (2015), Li et al. (2015), Placco et al. (2016), Sivarani et al. (2006), and Spite et al. (2013).

Against this background, and in particular the presence of significant numbers of stars having both low lithium and high carbon in the abundance range $-4.2 <$ [Fe/H] ≤ -3.0 in both main-sequence and LRGB samples, we are of the view that the same physical process most likely occurred in the two data sets.

[23]Given the [Fe/H] boundaries adopted in our Fig. 10 we have made a small change to the Mucciarelli et al. (2022) data for CS 0557–4840, for which they report [Fe/H] $= -4.44$. For convenience, we have adopted [Fe/H] $= 4.51$, which places it in the most metal-poor category; this may be acceptable to some extent given that we have previously derived [Fe/H] $= -4.75$ for this star (Norris et al. 2007; Norris 2018).

This paper has been typeset from a TEX/LATEX file prepared by the author.

Downloaded from https://academic.oup.com/mnras/article/522/1/1358/7095871 by guest on 27 April 2025

© 2023 The Author(s).
Published by Oxford University Press on behalf of Royal Astronomical Society. This is an Open Access article distributed under the terms of the Creative Commons Attribution License (http://creativecommons.org/licenses/by/4.0/), which permits unrestricted reuse, distribution, and reproduction in any medium, provided the original work is properly cited.